HHS Public Access

Author manuscript

Cell Rep. Author manuscript; available in PMC 2021 March 26.

Published in final edited form as:

Cell Rep. 2021 March 09; 34(10): 108827. doi:10.1016/j.celrep.2021.108827.

BOK controls apoptosis by Ca^{2+} transfer through ER-mitochondrial contact sites

Marcos A. Carpio[1,4], **Robert E. Means**[1,4], **Allison L. Brill**[2], **Alva Sainz**[1], **Barbara E. Ehrlich**[2,3], **Samuel G. Katz**[1,5,*]

[1]Department of Pathology, Yale School of Medicine, New Haven, CT 06525, USA

[2]Department of Cellular and Molecular Physiology, Yale School of Medicine, New Haven, CT 06525, USA

[3]Department of Pharmacology, Yale School of Medicine, New Haven, CT 06525, USA

[4]These authors contributed equally

[5]Lead contact

SUMMARY

Calcium transfer from the endoplasmic reticulum (ER) to mitochondria is a critical contributor to apoptosis. B cell lymphoma 2 (BCL-2) ovarian killer (BOK) localizes to the ER and binds the inositol 1,4,5-trisphosophate receptor (IP3R). Here, we show that BOK is necessary for baseline mitochondrial calcium levels and stimulus-induced calcium transfer from the ER to the mitochondria. Murine embryonic fibroblasts deficient for BOK have decreased proximity of the ER to the mitochondria and altered protein composition of mitochondria-associated membranes (MAMs), which form essential calcium microdomains. Rescue of the ER-mitochondrial juxtaposition with drug-inducible interorganelle linkers reveals a kinetic disruption, which when overcome in $Bok^{-/-}$ cells is still insufficient to rescue thapsigargin-induced calcium transfer and apoptosis. Likewise, a BOK mutant unable to interact with IP3R restores ER-mitochondrial proximity, but not ER-mitochondrial calcium transfer, MAM protein composition, or apoptosis. This work identifies the dynamic coordination of ER-mitochondrial contact by BOK as an important control point for apoptosis.

Graphical Abstract

*Correspondence: samuel.katz@yale.edu.

AUTHOR CONTRIBUTIONS

Conceptualization, M.A.C., B.E.E., and S.G.K.; methodology, M.A.C., R.E.M., A.L.B., and S.G.K.; validation, M.A.C., R.E.M., A.L.B., and A.S.; formal analysis, M.A.C. and R.E.M.; investigation, M.A.C., R.E.M., and A.S.; writing – original draft, M.A.C. and S.G.K.; writing – review & editing, M.A.C., R.E.M., A.L.B., B.E.E., and S.G.K.; visualization, M.A.C. and R.E.M.; supervision, B.E.E. and S.G.K.; project administration, S.G.K.; funding acquisition, S.G.K.

DECLARATION OF INTERESTS

The authors declare no competing interests.

SUPPLEMENTAL INFORMATION

Supplemental information can be found online at https://doi.org/10.1016/j.celrep.2021.108827.

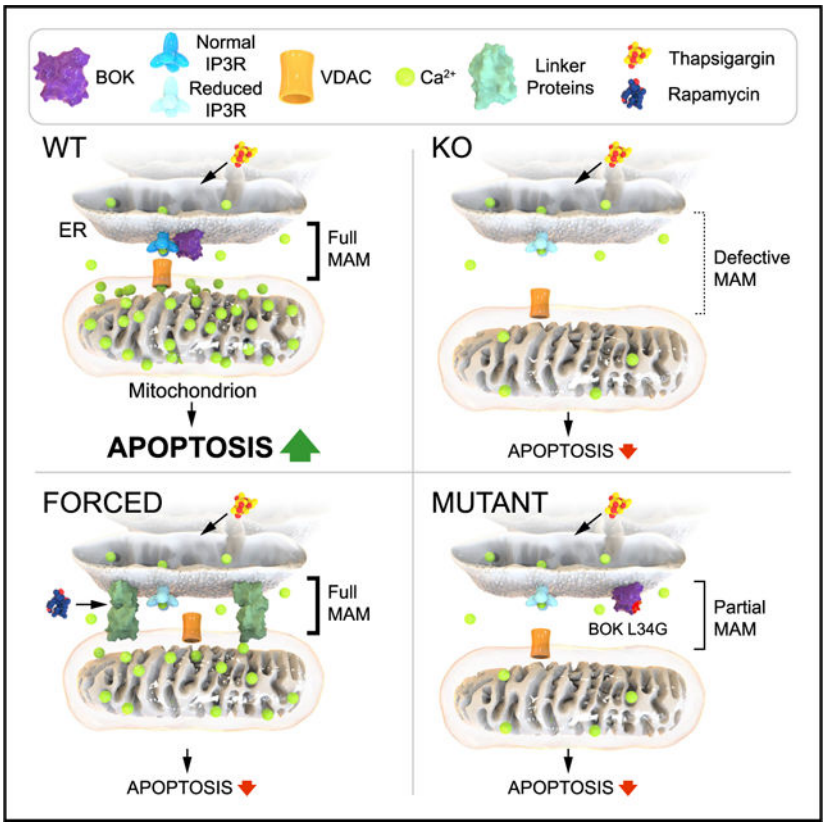

In brief

Carpio et al. demonstrate that the proapoptotic BCL-2 family member BOK is present in mitochondrial associated membranes (MAMs). The interaction of BOK with the IP3Rs is critical for its regulation of Ca^{2+} transfer to the mitochondria, ER-mitochondrial contact sites, and apoptosis.

INTRODUCTION

Approximately 5%–20% of the outer mitochondrial membrane (OMM) is in very close contact with the endoplasmic reticulum (ER), separated by no more than 10–30 nm (Csordás et al., 2006). This creates very specialized ER subdomains that, when biochemically purified, are known as mitochondria–associated ER membranes (MAMs) (Vance, 1990). Proteomic analyses have identified roughly 1,000–2,000 proteins within the MAMs, suggesting a rich signaling platform with a diverse set of functions (Poston et al., 2013; Zhang et al., 2011). Indeed, some of the tasks ascribed to ER-mitochondrial contact sites include the modulation of ER stress, calcium (Ca^{2+}) transfer, lipid biosynthesis and transfer, autophagosome initiation, and mitochondrial division (Marchi et al., 2014). Many of these pathways directly influence cell survival ultimately by affecting the intrinsic pathway of apoptosis mediated by the B cell lymphoma 2 (BCL-2) family of proteins at the OMM.

Ca^{2+} transfer is one of the best examples of a pathway that is critically dependent on the distance between the ER and the mitochondria and that leads to regulation of cell survival

(Csordás et al., 2010). The inositol 1,4,5-trisphosphate receptor (IP3R; particularly types 1 [IP3R1] and 3 [IP3R3]), the main ER Ca^{2+} release channel, and voltage-dependent anion channel (VDAC1), an OMM ion channel, exist in a complex with the chaperone glucose-regulated protein 75 kDa (GRP75) in the MAM fraction (Szabadkai et al., 2006). Altering the distance between the ER and mitochondria such that they are either too far apart or too close together to accommodate the IP3R results in reduced Ca^{2+} transfer efficiency (Csordás et al., 2010). However, the appropriate distance allows the assembly of these proteins in the MAMs to create a microdomain of high Ca^{2+} concentration, which is necessary to allow uptake by the low-affinity mitochondrial Ca^{2+} uniporter (MCU). Elevated levels of Ca^{2+} in the mitochondria result in permeability transition pore (PTP) opening, the release of cytochrome *c*, and cell death (Rizzuto et al., 2012).

BCL-2 family members control cell death not only by their canonical role in regulating OMM permeabilization but also by regulating the basal Ca^{2+} levels available for stress-induced ER Ca^{2+} release (Hardwick and Soane, 2013). Anti-apoptotic BCL-2, BCL-X_L, and MCL-1 each bind to the IP3R and enhance its leak of Ca^{2+} (Eckenrode et al., 2010; Monaco et al., 2012; White et al., 2005), whereas pro-apoptotic BAX and BAK are necessary to maintain ER Ca^{2+} stores (Scorrano et al., 2003). Although BAX and BAK do not directly bind to the IP3R, loss of BAX and BAK results in increased IP3R1-BCL-2 binding and IP3R1 hyperphos-phorylation, which makes it more sensitive to Ca^{2+} release by IP3 stimulation (Oakes et al., 2005).

BOK (BCL-2 Ovarian Killer), like several of the anti-apoptotic BCL-2 family members, also localizes to the ER where it binds to the IP3Rs (Echeverry et al., 2013; Schulman et al., 2013). However, BOK shares the most sequence similarity with the multi-domain, pro-apoptotic family members BAX and BAK. In agreement with prior overexpression studies, a recent study further demonstrated that like BAX and BAK, BOK is a proapoptotic effector that can induce membrane permeabilization and mitochondrial apoptosis (Llambi et al., 2016). In line with this finding, *Bok*$^{-/-}$ cells and mice exhibit partial protection from apoptosis due to ER stress agents such as the proteasome inhibitor bortezomib and the SERCA inhibitor thapsigargin (Carpio et al., 2015). Mechanistically, loss of BOK results in a disruption of the terminal unfolded protein response (UPR) that leads to apoptosis (Carpio et al., 2015). In addition, bortezomib stabilizes BOK, protecting it from constitutive ER-associated degradation (ERAD) due to ubiquitination (Llambi et al., 2016). Interestingly, BOK is also protected from ubiquitination and ERAD by binding to the IP3R (Schulman et al., 2016). Although BOK did not appear to have a major effect on IP3R Ca^{2+}-mobilizing function in permeabilized murine embryonic fibroblasts (MEFs) (Schulman et al., 2013) or lysophosphatidic acid (LPA)-induced uptake of cytosolic and mitochondrial Ca^{2+} (Schulman et al., 2019), BOK null neurons had impaired intracellular neuronal Ca^{2+} handling during NMDA excitotoxicity (D'Orsi et al., 2016).

In this study, we show that BOK is necessary to form a signaling platform between the ER and mitochondria that facilitates Ca^{2+} flux between these organelles. In the absence of BOK, MAMs are altered and ER Ca^{2+} channels are mis-localized. Moreover, whereas restoration of the ER-mitochondrial proximity with an inducible linker system does not rescue Ca^{2+} transfer or cell death, rescue with wild-type (WT) BOK does, and this rescue phenotype is

ablated with a BOK isoform that cannot bind to the IP3R. Taken together, our results highlight that BOK is required for proper mitochondria-ER contacts, the transfer of Ca^{2+}, and apoptosis.

RESULTS

BOK is necessary for the transfer of Ca^{2+} from the ER to mitochondria

To understand the significance of BOK binding to the IP3R, we measured intracellular Ca^{2+} in SV-40 immortalized MEFs (Figures 1 and S1). Live-cell high-resolution confocal microscopy was used to measure the relative Ca^{2+} levels in single cells expressing the fluorescent Ca^{2+} indicator proteins ER-LAR-GECO1, Cyto-RCaMP1h, and Mito-RCaMP1h for ER, cytoplasm, and mitochondrial measurements, respectively (Figure 1). In addition, confirmatory measurements were made with the indicator dyes Mag-Fluo-4 for the ER, Fluo-3 for the cytoplasm, and Rhod-2 for the mitochondria (Figure S1A). We first confirmed a high correlation between MitoTracker and Rhod-2, but not Mag-Fluo-4, and ER-Tracker with Mag-Fluo-4, but not Rhod-2, indicating appropriate localization (Figure S1B). At baseline, whereas WT and *Bok*$^{-/-}$ cells had equivalent levels of Ca^{2+} in the ER and cytoplasm, *Bok*$^{-/-}$ cells had diminished levels of mitochondrial Ca^{2+} (Figures 1 and S1A). The decreased level of Ca^{2+} in the *Bok*$^{-/-}$ mitochondria was not due to changes in mitochondrial membrane potential (Figure S1C). Loss of BOK partially protects cells from death induced by thapsigargin, an irreversible inhibitor of the SERCA pump responsible for uptake of Ca^{2+} from the cytosol into the ER lumen (Carpio et al., 2015). Thapsigargin (2 μM) caused equivalent levels of passive release of Ca^{2+} from ER stores in both WT and *Bok*$^{-/-}$ cells (Figures 1A and S1A). In addition, the transient increase in cytoplasmic Ca^{2+} induced by thapsigargin was similar in both WT and *Bok*$^{-/-}$ cells (Figures 1A and S1A). However, the uptake of mitochondrial Ca^{2+} in response to thapsigargin was significantly decreased in the *Bok*$^{-/-}$ cells compared with WT cells (Figures 1A and S1A). Unlike the similar decrease in induced mitochondrial Ca^{2+} uptake in the *Bax*$^{-/-}$*Bak*$^{-/-}$ MEFs (Oakes et al., 2005), this is not due to increased leak of Ca^{2+} from the ER (Figure S1D).

To more closely observe Ca^{2+} released by the IP3R, we measured Ca^{2+} after stimulation with 100 μM histamine, which signals through Gq-coupled receptors to generate IP3 (Figures 1B and S1A). *Bok*$^{-/-}$ cells had a reduced release of ER Ca^{2+} due to histamine stimulation compared with WT cells (Figures 1B and S1A). Similar to thapsigargin inhibition of the SERCA pump, histamine stimulation of the IP3R led to an equivalent transient cytoplasmic rise in Ca^{2+} in both WT and *Bok*$^{-/-}$ cells (Figures 1B and S1A), but a significantly reduced rise of mitochondrial Ca^{2+}in the *Bok*$^{-/-}$ cells (Figures 1B and S1B). As a second method to stimulate the IP3R, we treated cells with 10 μM ATP. Upon ATP stimulation, there is a decreased release of Ca^{2+} from the ER in the *Bok*$^{-/-}$ cells compared with WT cells (Figures 1C and S1A). Concomitantly, there is a transient rise of both cytoplasmic and mitochondrial Ca^{2+} upon ATP stimulation, which is decreased in the *Bok*$^{-/-}$ cells (Figures 1C and S1A). In summary, within the *Bok*$^{-/-}$ cells both SERCA inhibition and IP3R stimulation result in a reduced Ca^{2+} uptake in mitochondria, whereas IP3R stimulation also results in a reduced release of Ca^{2+} from the ER. These findings led us to explore the juxtaposition of the ER with the mitochondria in the *Bok*$^{-/-}$ cells.

Mitochondrial-ER contact points are decreased in the absence of BOK

As a first step to explore points of contact between the mitochondria and the ER that are important for Ca^{2+} transfer, we measured Ca^{2+} in cells stained with both Rhod-2 and Mag-Fluo-4. To maximize the potential to capture ER-mitochondrial overlap in the *Bok*$^{-/-}$ cells, we used a slightly wider z axis that resulted in the capture of some Mag-Fluo-4-positive ER on the edge of the nucleus. At a nominal axial resolution of <0.6 μm and at 5 frames/s, we noted points of overlap between the two Ca^{2+} compartments in WT cells that were greatly reduced in the *Bok*$^{-/-}$ cells (Figures 2A and S2A). Upon stimulation with thapsigargin, these points of overlap increased in the WT cells, but remained barely visible in the *Bok*$^{-/-}$ cells. Although the indicator dyes appear to be appropriately localized (Figure S1B), to attain more firm support we proceeded to measure ER-mitochondrial contacts by higher resolution methods. As a second method to observe ER-mitochondrial interaction that does not depend specifically on Ca^{2+}, we utilized confocal microscopy to image WT and *Bok*$^{-/-}$ cells that expressed either fluorescent proteins targeted to the mitochondria and ER (Figure 2B) or that were loaded with MitoTracker and ER-Tracker (Figure S2C). Again, the *Bok*$^{-/-}$ cells had decreased points of intersection between the two organelles compared with WT cells (Figures S2B and S2C). As a third method to quantify the distance between these two organelles, we used electron microscopy (EM) to measure the average proximity as well as the length where the distance was less than 15 nm, according to published protocols (Giacomello and Pellegrini, 2016). By both measurements, there was significantly decreased proximity between the ER and mitochondria in the *Bok*$^{-/-}$ cells compared with the WT cells (Figure 2C). The length and shape of the ER were similar between the WT and *Bok*$^{-/-}$ cells (Figure S2D).

MAM proteins are mis-localized in the absence of BOK

We next investigated the consequence of the decreased association between the ER and mitochondria on the localization of proteins known to concentrate in this subdomain. Co-localization of mitochondrial-resident MAM proteins with the ER protein calnexin (CNX), and between ER-resident MAM proteins with MitoTracker, was measured by confocal microscopy focusing on the protein of interest and using the same exposure for each pair of WT and *Bok*$^{-/-}$ staining (Figures 3 and S3). Of note, CNX staining looks similar to ER-Tracker (Figures S1B and S2C) and the CFP-ER reporter (Figure 2B). In agreement with the structural defect observed, we found decreased co-localization of known MAM protein FACL-4 with the mitochondria (Figure 3A). Moreover, proteins that mediate Ca^{2+} transport at MAMs (Hayashi and Su, 2007; Mendes et al., 2005; Szabadkai et al., 2006), including IP3R1 (Figure 3B), IP3R3 (Figure S3A), and Sigma-1 Receptor (Figure S3B), exhibit decreased co-localization with the mitochondria. In addition, at an equivalent exposure, we also note a decrease in total levels of IP3R1 (Figure 3B). IP3R2 showed minimal co-localization to the mitochondria and no difference in the *Bok*$^{-/-}$ cells (Figure 3C). ANT, which is an inner mitochondria membrane (IMM) protein (Vieira et al., 2000), showed minimal co-localization to the ER and no difference in the *Bok*$^{-/-}$ cells (Figure S3C). Although ANT has been shown to be associated with OMM proteins involved in MAMs, our inability to see a difference in its co-localization by microscopy may be due to the distance between the IMM and OMM of ~22–25 nm. Overall, the average Pearson correlation coefficient for WT and *Bok*$^{-/-}$ cells was 0.77 and 0.56 for FACL-4, 0.86 and 0.72 for IP3R1,

0.79 and 0.81 for IP3R3, 0.82 and 0.46 for Sigma-1 Receptor, 0.21 and 0.29 for ANT, and 0.36 and 0.41 for IP3R2, respectively.

As a second method to assess the localization of known MAM proteins, we performed biochemical purification from WT and *Bok*$^{-/-}$ SV-40 immortalized MEFs. In whole-cell extracts, we observed decreased IP3R1 and IP3R3 protein levels, but not other examined proteins, in the *Bok*$^{-/-}$ cells (Figures 4 and S4). We next separated the extract into bulk ER, mitochondrial, and MAM fractions. The purity of the mitochondrial fraction was verified by the selective localization of VDAC1 and ANT, whereas the bulk ER fraction was verified by calreticulin (CRT) and CNX. In agreement with the immunofluorescence, many proteins typically found in the MAM fraction in WT cells were decreased in the MAM fraction from the *Bok*$^{-/-}$ cells (e.g., IP3R1, IP3R3, and CRT). Although ANT is an IMM protein not seen to be proximal by immunofluorescence, there is a known biochemical association of ANT with the MAMs (Horner et al., 2015; Wang et al., 2018). Because of the concentration necessary to compare with the other fractions, ANT is too dilute to visualize in the whole-cell lysate (WCL). Interestingly, CNX and VDAC1 remained at normal expression levels within the MAM fraction in both WT and *Bok*$^{-/-}$ cells, suggesting that at least some MAM proteins are unaffected by BOK. However, a role for BOK in overall MAM structure is further supported by a distinct difference in mobility of purified MAMs on density centrifugation between WT and *Bok*$^{-/-}$ cells (Figure S4A). Thus, BOK is necessary for the appropriate localization of several proteins within ER-mitochondrial contact sites.

Restoration of ER-mitochondrial proximity without BOK does not rescue thapsigargin-induced Ca^{2+} transfer and apoptosis

We next attempted to reestablish the ER-mitochondrial proximity without BOK to see whether BOK's function in promoting the connection between the ER and mitochondria is sufficient to mediate its effects on apoptosis. To increase ER-mitochondrial connections, we transiently transfected the WT and *Bok*$^{-/-}$ cells with a set of drug-inducible fluorescent interorganelle linkers designed by the Hajnóczky and Scorrano laboratories (Csordás et al., 2010; Naon et al., 2016). Each of these systems expresses two proteins: one that contains the OMM-targeting sequence from mAKAP1 (34–63), FKBP12 (the 12-kDa FK506-binding protein), and a fluorescent protein and a second that contains the ER-targeting sequence from the human Sac1 phosphatase (521–587), FRB (FK506 rapamycin binding), and a different fluorescent protein. A short pulse of rapamycin can be used to dimerize FKBP12 and FRB, leading to narrowing of the ER-mitochondrial contacts and extension of the interface area. To measure proximity by FRET (fluorescence resonance energy transfer), the two fluorescent proteins used were yellow fluorescent protein (YFP) and cyan fluorescent protein (CFP). The one-plasmid system from the Scorrano laboratory contains a longer version of the ER-targeted protein that spans an ~15 nm distance between the ER and mitochondria (Figure 5), whereas the Hajnóczky two-plasmid system creates an ~5 nm distance between the two organelles (Figure S5). As a first step, without rapamycin, we treated WT and *Bok*$^{-/-}$ cells transiently transfected with these constructs with thapsigargin and measured FRET (Figures 5A and S5A). In agreement with our other findings, the *Bok*$^{-/-}$ cells had a much lower level of FRET at baseline than the WT cells. Moreover, upon stimulation with thapsigargin the WT cells had a mild increase in FRET, whereas the *Bok*$^{-/-}$

cells had a much smaller rise. Next, we added rapamycin to see whether we could induce proximity as measured by FRET within the *Bok*$^{-/-}$ cells (Figures 5B and S5B). Indeed, upon exposure of the cells to rapamycin, both WT and *Bok*$^{-/-}$ cells exhibited large increases in FRET to equivalent levels albeit with slower kinetics for the *Bok*$^{-/-}$ cells, taking ~4 min longer. This additional time likely not only reflects the increased starting distance between the two organelles in the *Bok*$^{-/-}$ cells that must be overcome but also implies that loss of BOK does not create a state wherein it is impossible to juxtapose the ER with the mitochondria.

Having established that we can rescue the ER-mitochondrial proximity in *Bok*$^{-/-}$ cells without BOK, we next sought to determine whether the apoptotic response to thapsigargin was also rescued. For this experiment, we used either the Scorrano system (Figure 5C) or the longer version of the Hajnóczky system that uses Pericam and red fluorescent protein (RFP), rather than CFP and YFP (Figure S5C). Both systems use an ER-targeted protein that creates an ~15 nm distance between the ER and mitochondria in order to accommodate the ~10 nm extension of the IP3R. Whereas WT cells that received the plasmids and rapamycin exhibited annexin V positivity in response to thapsigargin, BOK-disrupted cells continued to have low levels of annexin V regardless of the increased proximity of the ER and mitochondria (Figures 5C and S5C). Thus, the increased distance between the ER and mitochondria in the BOK-disrupted cells is not the only determinant preventing thapsigargin-induced apoptosis.

Given the inability to rescue apoptosis in the *Bok*$^{-/-}$ cells that had re-juxtaposition of the ER and mitochondria, we next sought to assess Ca^{2+} transfer. The long forms that accommodate the IP3R from the Scorrano laboratory and the Ca^{2+} indicator dyes have compatible fluorescent spectra. Cells transiently transfected with this plasmid were loaded with the indicated dyes, not treated or treated with rapamycin for 10 min, and then stimulated with thapsigargin (arrowhead, Figure 5D). Both WT and *Bok*$^{-/-}$ cells demonstrated equivalent release of ER Ca^{2+} (left column) and uptake of cytosolic Ca^{2+} (middle column) with or without rapamycin. Although rapamycin-induced linkage did not rescue stimulus-induced Ca^{2+} uptake in the mitochondria in the *Bok*$^{-/-}$ cells, it was sufficient to rescue the baseline levels of mitochondrial Ca^{2+} (right column). This suggests that ER-mitochondrial proximity without BOK is insufficient for coordinated mitochondrial Ca^{2+} uptake and thapsigargin-stimulated apoptosis.

Disruption of the BOK-IP3R interaction attenuates MAM protein composition, Ca^{2+} transfer from the ER to mitochondria, and apoptosis

To determine the significance of BOK's interaction with the IP3R, we rescued *Bok*$^{-/-}$ cell lines in a stable fashion with either WT BOK or a BOK L34G mutant described to not bind to the IP3R (Schulman et al., 2016). Co-immunoprecipitation confirmed that WT BOK bound to both IP3R1 and IP3R3 and that the L34G mutation greatly reduced its ability to bind either of them (Figure S6A). Whereas rescue of the *Bok*$^{-/-}$ cells with WT BOK restored the expression of MAM proteins, this was not observed with BOK L34G (Figures 6A and S6). Although there was equivalent overexpression of WT BOK and BOK L34G in WCLs (Figure S6I), BOK L34G was not able to localize to the MAMs. By contrast, when

we examined ER-mitochondrial proximity by EM, we found that BOK L34G is still significantly able to mediate the ER-mitochondrial contact (Figures 6B and 6C).

Stable expression of WT BOK restored the capacity of *Bok*$^{-/-}$ cells to maintain mitochondrial Ca^{2+} levels and respond to thapsigargin, histamine, and ATP (Figures 7A–7C and S7). However, BOK L34G did not restore the mitochondrial Ca^{2+} homeostasis or stimulus-induced Ca^{2+} flux. There was no difference in the mitochondrial potential between *Bok*$^{-/-}$ cell lines stably rescued with WT or L34G BOK (Figure S1C). Finally, given the known role for Ca^{2+} in contributing to apoptosis for BAX and BAK (Scorrano et al., 2003), we tested how the *Bok*$^{-/-}$ cells rescued with WT or L34G BOK responded to thapsigargin and bortezomib. As previously demonstrated (Carpio et al., 2015), the *Bok*$^{-/-}$ cells were partially resistant to apoptosis induced by thapsigargin or bortezomib, whereas stable expression of WT BOK rescued their response (Figures 7D and 7E). However, BOK L34G was not able to rescue the *Bok*$^{-/-}$ cells response to bortezomib or thapsigargin-induced cell death. This suggests that both bortezomib- and thapsigargin-induced ER stress requires BOK's ability to bind IP3R in promoting apoptosis.

DISCUSSION

Multiple BCL-2 family members play important roles in the regulation of Ca^{2+} homeostasis (Hardwick and Soane, 2013). For example, BCL-2, BCL-X_L, and MCL-1 each bind to the IP3R and enhance Ca^{2+} leak (Eckenrode et al., 2010; White et al., 2005), whereas BAX and BAK also partially localize to the ER and mediate apoptosis to select stimuli by virtue of their ability to regulate IP3R-mediated Ca^{2+} release, albeit not through direct IP3R interactions (Scorrano et al., 2003). Although a role has been proposed for BOK as an effector of mitochondrial outer membrane permeabilization similar to BAX and BAK (Llambi et al., 2016), its function in the regulation of ER Ca^{2+} remains unclear. Prior studies have demonstrated that the majority of BOK is tightly bound to the IP3R, which leads to their mutual protection from cleavage and degradation (Schulman et al., 2013, 2016). However, measurements of cytosolic Ca^{2+} showed either no significant changes in BOK-deficient fibroblasts stimulated with LPA (Schulman et al., 2013) or decreased peak cytosolic Ca^{2+} release in BOK-deficient cortical neurons stimulated with NMDA (D'Orsi et al., 2016). Mitochondrial Ca^{2+} uptake in fibroblasts stimulated with LPA also showed no significant changes in the BOK-deficient cells compared with WT cells (Schulman et al., 2019). However, only a single concentration of agonist was used, which may have evoked a maximal stimulation that could mask shifts in K_D. In addition, the studies of mitochondrial Ca^{2+} levels were performed in CRISPR-Cas9-BOK knockout (KO) MEFs without changes in IP3R protein levels.

In this study, we have further dissected Ca^{2+} dynamics within organelles to show that BOK is an effector of IP3R-mediated Ca^{2+} transfer from the ER to the mitochondria. In particular, BOK-deficient MEFs exhibit a baseline depression of mitochondrial Ca^{2+} and a decreased uptake of ER-released Ca^{2+} when the cells are stimulated by thapsigargin, a SERCA pump inhibitor, or histamine or ATP, IP3R agonists. We further show that BOK's regulation of Ca^{2+} transfer is likely essential for thapsigargin- and bortezomib-induced apoptosis. In looking at Ca^{2+} dynamics, we uncovered an unexpected role for BOK in maintaining

MAMs. Using immunofluorescence for both general and specific markers, biochemistry, EM, and FRET, we find that BOK null cells have a defect in the contacts between the ER and mitochondria. In addition, multiple MAM proteins are mis-localized by immunofluorescence and decreased by biochemistry in the *Bok*$^{-/-}$ cells.

Several potential mechanisms may contribute to the Ca^{2+} and ER-mitochondrial contact phenotypes observed in the *Bok*$^{-/-}$ cells. IP3R1, VDAC1, GRP75, and TG2 form a complex that regulates mitochondrial-ER contact sites (D'Eletto et al., 2018), and each of the IP3R isoforms support ER-mitochondrial contacts independently of Ca^{2+} flux (Bartok et al., 2019). We speculate that BOK-IP3R interactions may serve as a scaffolding complex that helps to maintain ER-mitochondrial contact. This hypothesis is supported by the recent finding of increased VDAC1-IP3R interactions in cells overexpressing MCL-1 and BOK transmembrane domains fused to a split Venus construct (Lucendo et al., 2020). Whereas BOK's role in the formation of ER-mitochondrial contacts appears important for the creation of Ca^{2+} microdomains, this is unlikely to be the sole mechanism by which BOK regulates Ca^{2+} transfer, because rescuing these contacts without BOK normalized baseline mitochondrial Ca^{2+} levels, but not thapsigargin-induced transfer of Ca^{2+} (Figure 5D). IP3R-isoform-specific functions might be important in BOK's ability to regulate Ca^{2+} dynamics. Whereas in some settings IP3R2 is the most effective in delivering Ca^{2+} to the mitochondria (Bartok et al., 2019), we find that loss of BOK affects localization of IP3R1 and IP3R3 more than IP3R2 (Figures 3 and S3). This may be due to cell-type-specific differences, as we have not detected IP3R2 localized to the MAM in kidney cells (Kuo et al., 2019), and others have identified IP3R1 as the main isoform responsible for mitochondrial Ca^{2+} uptake in hepatocytes (Feriod et al., 2017). In addition, although BOK has been reported to bind more strongly to IP3R1 and IP3R2 than IP3R3, we find that the L34G mutation disrupts BOK binding to both IP3R1 and IP3R3 (Figure S6). One possible role for BOK is protection of the IP3Rs stability, and their reduction in our *Bok*$^{-/-}$ cells may account for the reduced levels of mitochondrial Ca^{2+}. Another may be the reduction of the Ca^{2+}-binding protein CRT in MAMs, which may provide increased free Ca^{2+} for mitochondrial uptake. Alternatively, BOK may affect other components of the mitochondrial Ca^{2+} import system, such as the MCU, which contains regulatory elements that enhance pore opening in the presence of Ca^{2+}.

Although mitochondrial Ca^{2+} levels were uniformly diminished in response to all three stimuli, we did notice select impairment of ER Ca^{2+} release in *Bok*$^{-/-}$ cells when using IP3R agonists as opposed to the SERCA inhibitor. This may be due to plasma membrane Ca^{2+} channels in addition to the IP3R contributing to Ca^{2+} efflux in the presence of thapsigargin. ER Ca^{2+} release was similar for both IP3R agonists, but we only observed a decrease in cytoplasmic Ca^{2+} uptake in the *Bok*$^{-/-}$ cells stimulated with ATP. Mismatches between agonist-evoked Ca^{2+} depletion and cytosolic Ca^{2+} elevations may be due to differences in MAM localization, BOK binding affinity, and agonist-stimulating activity among the three IP3R isoforms. Furthermore, each agonist is likely to have differential effects on other Ca^{2+} channels throughout the cell, including at the plasma membrane.

Although cross-talk between the ER and mitochondria in the form of Ca^{2+} (Chami et al., 2008; Hayashi and Su, 2007; Mallilankaraman et al., 2012; Patron et al., 2014) or lipids

(Chipuk et al., 2012; Choi et al., 2007) is known to be important for apoptosis, relatively little is known about regulation of apoptosis by control of ER-mitochondrial proximity. Maintaining appropriate Ca^{2+} levels in the mitochondria is critical for cell death: enough Ca^{2+} must be transferred to maintain Ca^{2+}-sensitive citric-acid-cycle enzymes and ATP production (Pinton et al., 2008; Rutter and Rizzuto, 2000), but excessive Ca^{2+} transfer can lead to loss of mitochondrial membrane potential, cytochrome *c* release, and apoptosis (Hajnóczky et al., 2006; Szalai et al., 1999). Our finding that ER-mitochondrial proximity increases upon stress with thapsigargin (Figure 5A) supports the dynamic nature of these interactions in regulating apoptosis. Non-BCL-2 family members, such as MAPL and Drp1 (Prudent et al., 2015), have been shown to be required for cell death by their ability to stabilize ER-mitochondrial interactions. In addition, mitofusins are known to both regulate ER-mitochondrial contacts (de Brito and Scorrano, 2008) and mitochondrial morphology (Eura et al., 2003), the latter of which has been shown to affect susceptibility to apoptosis (Renault et al., 2015). Recently, the BCL-2 pro-apoptotic BH3-only protein BIK has been shown to increase the contact sites between the ER and mitochondria by promoting the association of ER-associated BAK with mitochondrial-associated DAPk1 (Mebratu et al., 2017). However, although ER-mitochondrial contacts may contribute to apoptosis, in the absence of BOK it is not sufficient, because the forced linking of the ER and mitochondria with rapamycin-induced binding did not rescue apoptosis in the $Bok^{-/-}$ cells (Figures 5C and S5C). One caveat is that the ER-mitochondrial proximity by the linker plasmids might not be appropriately organized; however, in that setting we might not have expected to see apoptosis proceed in the WT cells. Taken together, BOK regulates both ER-mitochondrial proximity and Ca^{2+} transfer between these two organelles, processes known to be important for apoptosis.

In addition to Ca^{2+} regulation, MAMs are important sites of action for the UPR (Carreras-Sureda et al., 2017; Verfaillie et al., 2012), mitochondrial fission (de Brito and Scorrano, 2008; Friedman et al., 2011), antiviral signaling (Horner et al., 2011), autophagy (Hamasaki et al., 2013), and lipid transfer and biosynthesis (Giacomello and Pellegrini, 2016; Vance, 1990, 1991). In fact, we have previously shown that $Bok^{-/-}$ cells have defects in the PERK pathway of the UPR (Carpio et al., 2015), and Schulman et al. (2019) have found that BOK regulates mitochondrial fusion. It is interesting to speculate that beyond the UPR, mitochondrial fusion, and Ca^{2+} transfer, BOK may participate in the regulation of additional MAM-related functions. Further analysis of BOK function within MAMs will be important to understand how MAMs coordinate a multitude of signaling pathways to determine cell fate and by what mechanisms and under which circumstances these may be therapeutically targeted.

STAR★METHODS

RESOURCE AVAILABILITY

Lead contact—Further information and requests for resources and reagents should be directed to and will be fulfilled by the lead contact, Samuel G. Katz (samuel.katz@yale.edu).

Materials availability—Cell lines generated in this study will be made available on request, but we may require a payment and/or a completed Materials Transfer Agreement if there is potential for commercial application.

Data and code availability—This study did not generate any unique datasets or code.

EXPERIMENTAL MODEL AND SUBJECT DETAILS

WT and *Bok*$^{-/-}$ murine embryonic fibroblast (MEF) pairs were derived at 13.5 days after conception from mating of *Bok*$^{+/-}$ heterozygous mice that had been backcrossed to C57BL/6J mice nine times. MEFs were immortalized with SV40 genomic DNA as described (Wei et al., 2001). MEFs were maintained in Dulbecco's modified Eagle's medium (DMEM) supplemented with 10% heat-inactivated fetal bovine serum (FBS), 4.5 g/L glucose, 4 mM L-glutamine, 200 units/ml penicillin and 100 ug/ml streptomycin. Stable cell lines were made by using lipofectamine to transfect *Bok*$^{-/-}$ MEFs with pMIG-FLAG-HA-WT BOK-IRES-GFP or pMIG-FLAG-HA-L34G BOK-IRES-GFP DNA. GFP positive cells were FACS sorted at multiple points weeks after transfection. Individual cell clones were plated at one cell per well and used for rescue experiments.

METHOD DETAILS

Live Cell Calcium Imaging—For imaging with the gene encoded Ca^{2+} indicators (ER-LAR-GECO1, mito-RCaMP1h and cyto-RCaMP1h), cells were cultured in Dulbecco's modified Eagle's medium (DMEM) (Life Technologies) supplemented with FBS (10%, Sigma–Aldrich) at 37°C in 5% CO_2. Cells were seeded in an 8-well Chamber Slide Nunc Lab-Tek (Thermo Fisher) and after 24 hr transiently transfected with plasmids using Lipofectamine 2000 (Life Technologies). Cells were imaged 24 hr after transfection in Hank's buffered salt solution (HBSS). Cells were stimulated with thapsigargin (2 μM), histamine (10 μM) or ATP (10 μM) (Sigma-Aldrich) and imaged with a Leica SP8 STED (Stimulated Emission Depletion) super resolution microscope using a UPLFLN 40 × , NA (numerical aperture), and 1.3 Plan-Apochromat objective. Cells were illuminated with 561 nm (for ER-LAR-GECO1) or 555 nm (for mito-RCaMP1h, and cyto-RCaMP1h) LED lights source and 580–630 nm and 600–650 nm emission filters, respectively. Ratiometric measurements and images were processed using Fiji (ImageJ) plugin and Time Series Analyzer (v3.0). All records were corrected for background fluorescence determined from regions outside cells. Fluorescence changes from regions of interest were expressed as F/F0, where F0 and F denote the average fluorescence at the start of the experiment (F0) and at each time point (F), respectively.

For the fluorescent Ca^{2+} dye sensors, the intracellular Ca^{2+} oscillations were measured as described (Carpio and Katz, 2019). Briefly, cells were treated with 5 μM sensor and 0.2% Pluronic F-127 acid at 37°C for 30 min. The cells were washed three times with 1x PBS and then Ca^{2+} was measured by exciting the indicator at the range of 450–500 nm (Fluo-3/AM, Mag-Fluo-4/AM) or 540–560 nm (Rhod-2/AM) for 3–5 min. Cells were then exposed to thapsigargin (2 μM), histamine (10 μM) or ATP (10 μM) and imaged for another 20–25 min. Cells were imaged by confocal microscopy with a Leica SP8 STED super resolution

microscope, using a UPLFLN 40 × , NA (numerical aperture), and 1.3 Plan-Apochromat objective. Pinholes were set for a nominal axial resolution of less than 0.6 μm.

Co-localization of Rhod-2 and Fluo-4 with ER- and Mito-Tracker in live cells— For dual-color imaging between ER-Tracker Green, ER-Tracker Red or MitoTracker Deep Red FM with Mag-Fluo-4 AM or Rhod-2 AM, WT and *Bok*$^{-/-}$ MEFs were seeded in an 8-well Chamber Slide Nunc Lab-Tek (Thermo Fisher). After 24 hr cells were rinsed with Hank's buffered salt solution (HBSS), and then incubated for 25 min at 37 C in HBSS prewarmed staining solution with 1 μM for ER-Tracker Green, 1 μM ER-Tracker Red or 100 nM MitoTracker Deep Red FM combined with 1 μM Mag-Fluo-4 AM or 1 μM Rhod-2 AM (supplemented with 0.02% Pluronic acid). Cells were rinsed three times in HBSS and then incubated for a further 30 min to allow complete de-esterification of intracellular AM esters. Cells were imaged using a Leica SP8 STED super resolution microscope using a HC PL APO 63x/1.40 OIL CS2 plan apochromat oil immersion objective and the following excitation LED light source/emission filters: 504/511 nm (for ER-TrackerTM Green), 587/615 nm (for ER-TrackerTM Red), 644/665 nm (for MitoTracker Deep Red FM), 490/517 nm (for Mag-Fluo-4 AM) and 552/581 nm (for Rhod-2 AM).

Co-localization using ER- and Mito-Tracker—WT and *Bok*$^{-/-}$ MEFs were rinsed with HBSS, and then incubated for 20 minutes at 37 C in prewarmed staining solution (HBSS with 1 μM for ER-Tracker™ Green and 100 nM MitoTracker® Deep Red FM). The cells were rinsed three times with probe-free HBSS and then fixed with 4% formaldehyde for 15 minutes at 37 C. After two 5-minute washes with PBS the cells were mounted and then analyzed by confocal microscopy.

Co-localization using pShooter-Mito-GFP and mRFP-FRB-9x-ER—DNA was introduced into WT and *Bok*$^{-/-}$ MEFs using a Maxcyte ATX electroporator. In brief, 2.5×10^6 cells were washed in Maxcyte HyClone buffer, resuspended in the same buffer containing 3 μg each of pShooter-Mito-GFP and mRFP-FRB-9x-ER DNA, and electroporated with optimization protocol 2. Cells were then seeded into 4-well chamber slides at 6×10^4 cells per well. Two days post-electroporation cells were washed with HBSS followed by fixation with 2% paraformaldehyde containing 1% glycerol for 30 min. in the dark at room temperature. Cells were then washed with dH_2O and mounted with ProLong Diamond antifade medium containing SYTOX Deep Red nuclei stain. Slides were then visualized on a Zeiss LSM 880 with Airyscan microscope using discreet excitation and emission filters for each fluorophore (GFP: BP420–480 & LP495–550, RFP: BP495–550 & LP570, Deep Red: BP570–620 &LP 660). Quantification of colocalization used the Zeiss Zen Black software to calculate GFP+RFP+/GFP+ pixels.

Immunofluorescence—For dual-color imaging between MitoTracker Deep Red FM and ER-targeted antibodies, WT and *Bok*$^{-/-}$ MEFs were plated on glass coverslips at 60% confluence and then incubated for 24 h. Cells were rinsed with HBSS, incubated for 25 minutes at 37 C in HBSS prewarmed staining solution with 100 nM MitoTracker Deep Red FM, rinsed three times in HBSS, and then incubated for a further 30 minutes. Cells were fixed with 3% formaldehyde and 4% sucrose in PBS for 30 min at room temperature,

permeabilized with 0.2% Triton X-100 in PBS for 10 min, and then treated with 5% bovine serum albumin (BSA) for 1 hr prior to addition of antibodies. Cells were incubated overnight at 4°C with the indicated primary antibody, rinsed three times with PBS, and then incubated for 1 hr at room temperature with PBS containing 1% BSA with the secondary antibody. Alexa Fluor 488-conjugated goat anti-mouse IgG secondary antibody (1:1,000; Molecular Probes) for FCL4, IP3R-I, IP3R-II, IP3R-3 and CNX antibodies. Alexa Fluor 546-conjugated goat anti-mouse IgG (1:1,000) for Sigma-1 Receptor and ANT antibodies. Cells were imaged using a Leica SP8 STED super resolution microscope using a HC PL APO 63x/1.40 OIL CS2 plan apochromat oil immersion objective and the following excitation LED light source/emission filters: 490/517 nm (for Alexa Fluor 488), 550/581 nm (for Alexa Fluor 546) and 644/665 nm (for MitoTracker Deep Red FM). TO-PRO0®−3 far red-fluorescent counterstain was used to stain cellular nuclei.

MAM isolation—MAMs (Mitochondrial associated membranes) were isolated from MEFs as described (Wieckowski et al., 2009). Six 150 mm tissue-culture dishes of MEFs were trypsinized with 0.25% trypsin for 5 minutes at 37°C. Two volumes of DMEM with 10% FBS were added prior to pelleting at 600 g for 5 minutes. Pellets were washed in 1xPBS followed by re-pelleting and resuspension in ice-cold buffer 1 (225 mM mannitol, 75 mM sucrose, 0.1 mM EGTA and 30 mM Tris–HCl pH 7.4). Cells were needle homogenized by passing 10 times each, successively through 20 Ga, 23 Ga, and 25 Ga needles. Lysates were centrifuged at 600 g for 5 min at 4°C and the pellet was discarded. The supernatant was centrifuged at 7,000 g for 10 min at 4°C. The supernatant was collected as the cytosolic fraction containing lysosomes and microsomes. To produce purified ER proteins, the supernatant was diluted with ice-cold buffer 1 and then centrifuged at 100,000 g for 60 min at 4°C.

The pellet from the previous 7,000 g spin, containing mitochondria and MAMs, was re-suspended in 20 mL of ice-cold buffer 2 (225 mM mannitol, 75 mM sucrose, and 30 mM Tris–HCl pH 7.4) and centrifuged twice (once at 7,000 g and once at 10,000 g for 10 min at 4°C) to remove microsomal contamination. The supernatant was discarded and the crude mitochondrial pellet re-suspended in 2 mL of ice-cold MRB buffer (250 mM mannitol, 5 mM HEPES (pH 7.4), and 0.5 mM EGTA). This was added on top of 8 mL of Percoll medium (225 mM mannitol, 25 mM HEPES (pH 7.4), 1 mM EGTA, and 30% Percoll) in a 14 mL thin-wall, Polyallomer ultracentrifuge tube and centrifuged at 95,000 g for 30 min at 4°C. A dense band containing purified mitochondria was localized at the bottom of the ultracentrifuge tube just above a Percoll pellet, while MAMs were visible as a diffuse white band located approximately half-way up the tube. Both were collected from the Percoll gradient with a Pasteur pipette, diluted with MRB, and re-centrifuged at 100,000 g for 60 min at 4°C to remove Percoll contamination.

Immunoblotting assays—Total protein concentration was quantitated with the BCA protein assay kit (Thermo Scientific). Equal quantities of proteins from each fraction were separated by SDS-PAGE (Bio-Rad Mini-PROTEAN® TGX Stain-Free™), transferred onto a PVDF membrane, blocked with 5% milk in TBS-Tween, and detected with the indicated primary antibodies incubated over-night at 4°C followed by incubation for 1 hr with the

appropriate HRP-linked secondary (either mouse or rabbit) at a 1:6000 dilution. For IP3R1, 20 μg protein was loaded, rabbit primary antibody (Invitrogen) was used at 1:2000. For IP3R3, 20 μg protein was loaded, mouse primary antibody (BD Biosciences) was used at 1:4000. For CRT, 10 μg of protein was loaded, mouse primary antibody (BD Biosciences) was used at 1:6000. For CNX, 10 μg of protein was loaded, mouse primary antibody (Santa Cruz) was used at 1:2000. For ANT, 40 μg protein was loaded, mouse primary antibody (Abcam) was used at 1:1000. For VDAC, 40 μg of protein was loaded, rabbit primary antibody (Thermo-Fisher) was used at 1:1000. For BOK, 20 μg of protein was loaded, rabbit primary antibody (Abcam) was used at 1:5000. The PVDF membrane was visualized with SuperSignal® West Pico Chemiluminescent Substrate (Thermo Scientific) or Kindle Biosciences KwikQuant using a Bio-Rad ChemiDoc MP.

Transmission Electron Microscopy—MEFs were fixed with 2.5% glutaraldehyde in 0.1 M sodium cacodylate buffer at pH 7.4 for 1 hr at room temperature and further processed and imaged by the Yale Electron Microscopy Core Facility as described (Lee et al., 2014).

Mitochondrial Potential—Mitochondrial potential was measured using the Mitostatus TMRE kit following the manufacturer's instructions.

Live Cell FRET imaging—We thank G. Csordas, G. Hajnóczky, and L. Scorrano, for sharing their rapamycin-inducible fluorescent interorganelle constructs. The Hajnóczky construct is a two plasmid system; one of which contains the ER targeting sequence from the human Sac1 phosphatase (521–587), FRB and CFP, and the second of which contains the OMM targeting sequence from mAKAP1 (34–63), FKBP12 and YFP (Csordás et al., 2010). The FEMP construct from L. Scorrano is a modified one-plasmid system based on the Hajnóczky construct (Naon et al., 2016). WT and $Bok^{-/-}$ cells were transfected with plasmids 24 hr before FRET measurement. A Leica SP8 STED (Stimulated Emission Depletion) super resolution microscope was used to record the fluorescence of CFP and YFP. The 488 Argon laser was selected to the donor excitation and a line corresponding to the acceptor excitation was 543 nm laser. The laser line was set up at 100% for the acceptor bleaching, a region of interest (ROI) was selected corresponding to the bleaching area and the region where the FRET efficiency was calculated. A time course of CFP and FRET fluorescence during induction of the linkage by rapamycin was measured and then a ratio FRET/CFP was calculated.

Co-immunoprecipitation assays—WT BOK and BOK L34G full length isoforms were immunoprecipitated using an anti-FLAG antibody and standard protocols. In brief, 3 μL of anti-FLAG monoclonal antibody was incubated for 1 hr at 4°C with 25 μL of Protein G Sepharose® 4 Fast Flow (GE17-0618-01) in 1 mL of RIPA buffer. The suspension was briefly centrifuged and the pellet washed twice with RIPA buffer. Then, cell lysate (300–500 μg of protein) was added to the suspension and the mixture was rotated overnight at 4°C. The suspension was briefly centrifuged and the supernatant discarded. The protein G Sepharose/anti-FLAG-BOK or G Sepharose/anti-FLAG-BOK L34G complexes were washed 5 times with 500 μL of RIPA buffer prior to the addition of Laemmli sample buffer.

Samples were subjected to WB using IP3R1 and IP3R3 antibodies to identify co-immunoprecipitation of proteins with the BOK isoforms.

XTT assay—Cells were plated at 5,000 cells per well in a clear-bottom 96 well plate. Approximately 24 hr post-plating, thapsigargin or bortizimab were added to the indicated final concentrations and cells were incubated for a further 24 hr. Measurement of cell viability was performed by XTT Cell Viability Assay (Cell Signaling Technology) according to the manufacturer's protocol.

Annexin V assay—Cells were plated in 6 well dishes and incubated over-night. The following day cells were either mock transfected or transfected with FEMP or both the RFP-ER-targeting and Pericam-mitochondria-targeting plasmids. After an additional 24 hr incubation, cells were treated with 0 or 100 nM rapamycin for 10 min at 37°C. Media was replaced with 2 μM thapsigargin or DMSO. After an additional 24 hr incubation, cells were detached from the plate using 0.25% trypsin, washed twice in complete medium and re-suspended in annexin V-staining buffer (BioLegend). Cells were then stained with PE/Cy7 or APC annexin V for approximately 15 min before analysis on a Stratedigm-13 or CytoFlex flow cytometer. Cells were analyzed for percentage of population with annexin V positivity. Transfected cells were additionally gated for either CFP and YFP or Pericam and RFP positivity before examining cells for PE/Cy7 or APC, respectively.

QUANTIFICATION AND STATISTICAL ANALYSIS

The Ca^{2+} fluorescence intensity ratio (Ft/F0) was plotted as a function of time. To quantify the fluorescence intensity during the time lapse we employed ImageJ software with Times Series Analyzer V3 plugin. Approximately 160 – 200 ROI (Regions of interest), each from one cell, were chosen from three independent experiments. The mean from one representative experiment is plotted in each graph in Figures 1, S1, and S7. The plots in Figure 7 and the insets in Figure S1 are of the mean ± standard deviation (SD) at the maximal difference. P values were determined by one-way ANOVA.

A quantification of percentage of colocalization for Ca^{2+}, immunostains with antibodies, and CNX or MitoTracker was performed using the colocalization manager plugin included in ImageJ 1.46R. Number of tests and significance are described in the figure legends. A Pearson correlation coefficient was performed for all the combination of antibodies with the MitoTracker using Prism 7 software.

Western blot band intensities were quantified by Biorad software and presented as the mean ± standard deviation (SD) of at least three independent experiments. A Student's t test for differences between the groups was considered statistically significant at $p < 0.05$.

For electron microscopy images, distance and length of contact sites between endoplasmic reticulum and mitochondria and length and circularity of ER were performed using an ROI manager plugin by ImageJ 1.46R software. Briefly, the images were converted to 8-bit and processed creating specific ROI for endoplasmic reticulum and mitochondria shape in different fields. Then, the distance between both organelles was obtained for each 10 nm along the interface between the ER and mitochondria taking a threshold of maximum

distance (200 nm). To quantify the length of contact sites a threshold of minimum distance between ER and Mito was established (40 nm) and then the distance along that proximity was measured. The endoplasmic reticulum circularity was measured using the circularity plugin included in ImageJ 1.46R. Number of tests and significance are described in the figure legends.

For FRET, calculations were made for at least 50 ROIs (3 experiments, 7–15 cells in each). An extra ROI was selected outside the cell in order to measure the background. If the background values were high, these values would need to be subtracted from the donor pre- and post- bleaching in order to compensate for the background noise. Another control was to determine YFP and CFP crosstalk into the FRET channel.

For cells expressing YFP construct only, YFPex/YFPem, CFPex/CFPem, CFPex/YFPem was measured. Any signal in the FRET channel (CFPex/YFPem) was therefore due to crosstalk of the YFP signal into this channel. This crosstalk (measured as a ratio of the CFP/YFP signal to the YFP/YFP signal) was subtracted from the FRET signal measured in experimental cells. In addition, for cells expressing the CFP construct only, YFPex/YFPem, CFPex/CFPem, CFPex/YFPem was measured. Any signal in the FRET channel (CFPex/YFPem) was due to crosstalk of the CFP signal into this channel. This crosstalk (measured as a ratio of the CFP/YFP signal to the CFP/CFP signal) was also subtracted from the FRET signal measured in experimental cells. The efficiency of FRET was calculated by: FRET eff = (Dpost-Dpre)/Dpost; where Dpost is the fluorescence intensity of the Donor after acceptor photobleaching, and Dpre is the fluorescence intensity of the Donor before acceptor photobleaching. Mean FRET efficiencies were then reported ± standard error.

For cell death determination by XTT assay or Annexin V flow cytometry, data is presented as the mean ± standard error of the mean (SEM) of three independent experiments as indicated in the figure legends.

Supplementary Material

Refer to Web version on PubMed Central for supplementary material.

ACKNOWLEDGMENTS

We thank I. Kuo for helpful advice, Jessica Su for technical support, Al Mennone in the Yale Confocal microscopy facility, Xinran Liu in the EM facility, and the fluorescence-activated cell sorting (FACS) cores for technical assistance. This work was supported by NIH grant 1R01HL131793, F31DK118836, a Gabrielle's Angel Foundation award, and the March of Dimes Basil O'Connor Starter Scholar research award.

REFERENCES

Bartok A, Weaver D, Golenár T, Nichtova Z, Katona M, Bánsághi S, Alzayady KJ, Thomas VK, Ando H, Mikoshiba K, et al. (2019). IP_3 receptor isoforms differently regulate ER-mitochondrial contacts and local calcium transfer. Nat. Commun 10, 3726. [PubMed: 31427578]

Carpio MA, and Katz SG (2019). Methods to Probe Calcium Regulation by BCL-2 Family Members. Methods Mol. Biol 1877, 173–183. [PubMed: 30536006]

Carpio MA, Michaud M, Zhou W, Fisher JK, Walensky LD, and Katz SG (2015). BCL-2 family member BOK promotes apoptosis in response to endoplasmic reticulum stress. Proc. Natl. Acad. Sci. USA 112, 7201–7206. [PubMed: 26015568]

Carreras-Sureda A, Pihán P, and Hetz C (2017). The Unfolded Protein Response: At the Intersection between Endoplasmic Reticulum Function and Mitochondrial Bioenergetics. Front. Oncol 7, 55. [PubMed: 28421160]

Chami M, Oulès B, Szabadkai G, Tacine R, Rizzuto R, and Paterlini-Bréchot P (2008). Role of SERCA1 truncated isoform in the proapoptotic calcium transfer from ER to mitochondria during ER stress. Mol. Cell 32, 641–651. [PubMed: 19061639]

Chipuk JE, McStay GP, Bharti A, Kuwana T, Clarke CJ, Siskind LJ, Obeid LM, and Green DR (2012). Sphingolipid metabolism cooperates with BAK and BAX to promote the mitochondrial pathway of apoptosis. Cell 148, 988–1000. [PubMed: 22385963]

Choi SY, Gonzalvez F, Jenkins GM, Slomianny C, Chretien D, Arnoult D, Petit PX, and Frohman MA (2007). Cardiolipin deficiency releases cytochrome c from the inner mitochondrial membrane and accelerates stimuli-elicited apoptosis. Cell Death Differ. 14, 597–606. [PubMed: 16888643]

Csordás G, Renken C, Várnai P, Walter L, Weaver D, Buttle KF, Balla T, Mannella CA, and Hajnóczky G (2006). Structural and functional features and significance of the physical linkage between ER and mitochondria. J. Cell Biol 174, 915–921. [PubMed: 16982799]

Csordás G, Várnai P, Golenár T, Roy S, Purkins G, Schneider TG, Balla T, and Hajnóczky G (2010). Imaging interorganelle contacts and local calcium dynamics at the ER-mitochondrial interface. Mol. Cell 39, 121–132. [PubMed: 20603080]

de Brito OM, and Scorrano L (2008). Mitofusin 2 tethers endoplasmic reticulum to mitochondria. Nature 456, 605–610. [PubMed: 19052620]

D'Eletto M, Rossin F, Occhigrossi L, Farrace MG, Faccenda D, Desai R, Marchi S, Refolo G, Falasca L, Antonioli M, et al. (2018). Transglutaminase Type 2 Regulates ER-Mitochondria Contact Sites by Interacting with GRP75. Cell Rep. 25, 3573–3581.e4. [PubMed: 30590033]

D'Orsi B, Engel T, Pfeiffer S, Nandi S, Kaufmann T, Henshall DC, and Prehn JH (2016). Bok Is Not Pro-Apoptotic But Suppresses Poly ADP-Ribose Polymerase-Dependent Cell Death Pathways and Protects against Excitotoxic and Seizure-Induced Neuronal Injury. J. Neurosci 36, 4564–4578. [PubMed: 27098698]

Echeverry N, Bachmann D, Ke F, Strasser A, Simon HU, and Kaufmann T (2013). Intracellular localization of the BCL-2 family member BOK and functional implications. Cell Death Differ. 20, 785–799. [PubMed: 23429263]

Eckenrode EF, Yang J, Velmurugan GV, Foskett JK, and White C (2010). Apoptosis protection by Mcl-1 and Bcl-2 modulation of inositol 1,4,5-trisphosphate receptor-dependent Ca2+ signaling. J. Biol. Chem 285, 13678–13684. [PubMed: 20189983]

Eura Y, Ishihara N, Yokota S, and Mihara K (2003). Two mitofusin proteins, mammalian homologues of FZO, with distinct functions are both required for mitochondrial fusion. J. Biochem 134, 333–344. [PubMed: 14561718]

Feriod CN, Oliveira AG, Guerra MT, Nguyen L, Richards KM, Jurczak MJ, Ruan HB, Camporez JP, Yang X, Shulman GI, et al. (2017). Hepatic Inositol 1,4,5 Trisphosphate Receptor Type 1 Mediates Fatty Liver. Hepatol. Commun 1, 23–35. [PubMed: 28966992]

Friedman JR, Lackner LL, West M, DiBenedetto JR, Nunnari J, and Voeltz GK (2011). ER tubules mark sites of mitochondrial division. Science 334, 358–362. [PubMed: 21885730]

Giacomello M, and Pellegrini L (2016). The coming of age of the mitochondria-ER contact: a matter of thickness. Cell Death Differ. 23, 1417–1427. [PubMed: 27341186]

Hajnóczky G, Csordás G, Das S, Garcia-Perez C, Saotome M, Sinha Roy S, and Yi M (2006). Mitochondrial calcium signalling and cell death: approaches for assessing the role of mitochondrial Ca2+ uptake in apoptosis. Cell Calcium 40, 553–560. [PubMed: 17074387]

Hamasaki M, Furuta N, Matsuda A, Nezu A, Yamamoto A, Fujita N, Oomori H, Noda T, Haraguchi T, Hiraoka Y, et al. (2013). Autophagosomes form at ER-mitochondria contact sites. Nature 495, 389–393. [PubMed: 23455425]

Hardwick JM, and Soane L (2013). Multiple functions of BCL-2 family proteins. Cold Spring Harb. Perspect. Biol 5, a008722. [PubMed: 23378584]

Hayashi T, and Su TP (2007). Sigma-1 receptor chaperones at the ER-mitochondrion interface regulate Ca(2+) signaling and cell survival. Cell 131, 596–610. [PubMed: 17981125]

Horner SM, Liu HM, Park HS, Briley J, and Gale M Jr. (2011). Mitochondrial-associated endoplasmic reticulum membranes (MAM) form innate immune synapses and are targeted by hepatitis C virus. Proc. Natl. Acad. Sci. USA 108, 14590–14595. [PubMed: 21844353]

Horner SM, Wilkins C, Badil S, Iskarpatyoti J, and Gale M Jr. (2015). Proteomic analysis of mitochondrial-associated ER membranes (MAM) during RNA virus infection reveals dynamic changes in protein and organelle trafficking. PLoS ONE 10, e0117963. [PubMed: 25734423]

Kuo IY, Brill AL, Lemos FO, Jiang JY, Falcone JL, Kimmerling EP, Cai Y, Dong K, Kaplan DL, Wallace DP, et al. (2019). Polycystin 2 regulates mitochondrial Ca^{2+} signaling, bioenergetics, and dynamics through mitofusin 2. Sci. Signal 12, eaat7397. [PubMed: 31064883]

Lee I, Tiwari N, Dunlop MH, Graham M, Liu X, and Rothman JE (2014). Membrane adhesion dictates Golgi stacking and cisternal morphology. Proc. Natl. Acad. Sci. USA 111, 1849–1854. [PubMed: 24449908]

Llambi F, Wang YM, Victor B, Yang M, Schneider DM, Gingras S, Parsons MJ, Zheng JH, Brown SA, Pelletier S, et al. (2016). BOK Is a Non-canonical BCL-2 Family Effector of Apoptosis Regulated by ER-Associated Degradation. Cell 165, 421–433. [PubMed: 26949185]

Lucendo E, Sancho M, Lolicato F, Javanainen M, Kulig W, Leiva D, Duart G, Andreu-Fernández V, Mingarro I, and Orzáez M (2020). Mcl-1 and Bok transmembrane domains: Unexpected players in the modulation of apoptosis. Proc. Natl. Acad. Sci. USA 117, 27980–27988. [PubMed: 33093207]

Mallilankaraman K, Doonan P, Cárdenas C, Chandramoorthy HC, Müller M, Miller R, Hoffman NE, Gandhirajan RK, Molgó J, Birnbaum MJ, et al. (2012). MICU1 is an essential gatekeeper for MCU-mediated mitochondrial Ca(2+) uptake that regulates cell survival. Cell 151, 630–644. [PubMed: 23101630]

Marchi S, Patergnani S, and Pinton P (2014). The endoplasmic reticulum-mitochondria connection: one touch, multiple functions. Biochim. Biophys. Acta 1837, 461–469. [PubMed: 24211533]

Mebratu YA, Leyva-Baca I, Wathelet MG, Lacey N, Chand HS, Choi AMK, and Tesfaigzi Y (2017). Bik reduces hyperplastic cells by increasing Bak and activating DAPk1 to juxtapose ER and mitochondria. Nat. Commun 8, 803. [PubMed: 28986568]

Mendes CC, Gomes DA, Thompson M, Souto NC, Goes TS, Goes AM, Rodrigues MA, Gomez MV, Nathanson MH, and Leite MF (2005). The type III inositol 1,4,5-trisphosphate receptor preferentially transmits apoptotic Ca2+ signals into mitochondria. J. Biol. Chem 280, 40892–40900. [PubMed: 16192275]

Monaco G, Beckers M, Ivanova H, Missiaen L, Parys JB, De Smedt H, and Bultynck G (2012). Profiling of the Bcl-2/Bcl-X(L)-binding sites on type 1 IP(3) receptor. Biochem. Biophys. Res. Commun 428, 31–35. [PubMed: 23058917]

Naon D, Zaninello M, Giacomello M, Varanita T, Grespi F, Lakshminaranayan S, Serafini A, Semenzato M, Herkenne S, Hernández-Alvarez MI, et al. (2016). Critical reappraisal confirms that Mitofusin 2 is an endoplasmic reticulum-mitochondria tether. Proc. Natl. Acad. Sci. USA 113, 11249–11254. [PubMed: 27647893]

Oakes SA, Scorrano L, Opferman JT, Bassik MC, Nishino M, Pozzan T, and Korsmeyer SJ (2005). Proapoptotic BAX and BAK regulate the type 1 inositol trisphosphate receptor and calcium leak from the endoplasmic reticulum. Proc. Natl. Acad. Sci. USA 102, 105–110. [PubMed: 15613488]

Patron M, Checchetto V, Raffaello A, Teardo E, Vecellio Reane D, Mantoan M, Granatiero V, Szabò I, De Stefani D, and Rizzuto R (2014). MICU1 and MICU2 finely tune the mitochondrial Ca2+ uniporter by exerting opposite effects on MCU activity. Mol. Cell 53, 726–737. [PubMed: 24560927]

Pinton P, Giorgi C, Siviero R, Zecchini E, and Rizzuto R (2008). Calcium and apoptosis: ER-mitochondria Ca2+ transfer in the control of apoptosis. Oncogene 27, 6407–6418. [PubMed: 18955969]

Poston CN, Krishnan SC, and Bazemore-Walker CR (2013). In-depth proteomic analysis of mammalian mitochondria-associated membranes (MAM). J. Proteomics 79, 219–230. [PubMed: 23313214]

Prudent J, Zunino R, Sugiura A, Mattie S, Shore GC, and McBride HM (2015). MAPL SUMOylation of Drp1 Stabilizes an ER/Mitochondrial Platform Required for Cell Death. Mol. Cell 59, 941–955. [PubMed: 26384664]

Renault TT, Floros KV, Elkholi R, Corrigan KA, Kushnareva Y, Wieder SY, Lindtner C, Serasinghe MN, Asciolla JJ, Buettner C, et al. (2015). Mitochondrial shape governs BAX-induced membrane permeabilization and apoptosis. Mol. Cell 57, 69–82. [PubMed: 25482509]

Rizzuto R, De Stefani D, Raffaello A, and Mammucari C (2012). Mitochondria as sensors and regulators of calcium signalling. Nat. Rev. Mol. Cell Biol 13, 566–578. [PubMed: 22850819]

Rutter GA, and Rizzuto R (2000). Regulation of mitochondrial metabolism by ER Ca2+ release: an intimate connection. Trends Biochem. Sci 25, 215–221. [PubMed: 10782088]

Schulman JJ, Wright FA, Kaufmann T, and Wojcikiewicz RJ (2013). The Bcl-2 protein family member Bok binds to the coupling domain of inositol 1,4,5-trisphosphate receptors and protects them from proteolytic cleavage. J. Biol. Chem 288, 25340–25349. [PubMed: 23884412]

Schulman JJ, Wright FA, Han X, Zluhan EJ, Szczesniak LM, and Wojcikiewicz RJ (2016). The Stability and Expression Level of Bok Are Governed by Binding to Inositol 1,4,5-Trisphosphate Receptors. J. Biol. Chem 291, 11820–11828. [PubMed: 27053113]

Schulman JJ, Szczesniak LM, Bunker EN, Nelson HA, Roe MW, Wagner LE 2nd Yule DI, and Wojcikiewicz RJH (2019). Bok regulates mitochondrial fusion and morphology. Cell Death Differ. 26, 2682–2694. [PubMed: 30976095]

Scorrano L, Oakes SA, Opferman JT, Cheng EH, Sorcinelli MD, Pozzan T, and Korsmeyer SJ (2003). BAX and BAK regulation of endoplasmic reticulum Ca2+: a control point for apoptosis. Science 300, 135–139. [PubMed: 12624178]

Szabadkai G, Bianchi K, Várnai P, De Stefani D, Wieckowski MR, Cavagna D, Nagy AI, Balla T, and Rizzuto R (2006). Chaperone-mediated coupling of endoplasmic reticulum and mitochondrial Ca2+ channels. J. Cell Biol 175, 901–911. [PubMed: 17178908]

Szalai G, Krishnamurthy R, and Hajnóczky G (1999). Apoptosis driven by IP(3)-linked mitochondrial calcium signals. EMBO J. 18, 6349–6361. [PubMed: 10562547]

Vance JE (1990). Phospholipid synthesis in a membrane fraction associated with mitochondria. J. Biol. Chem 265, 7248–7256. [PubMed: 2332429]

Vance JE (1991). Newly made phosphatidylserine and phosphatidylethanol-amine are preferentially translocated between rat liver mitochondria and endoplasmic reticulum. J. Biol. Chem 266, 89–97. [PubMed: 1898727]

Verfaillie T, Rubio N, Garg AD, Bultynck G, Rizzuto R, Decuypere JP, Piette J, Linehan C, Gupta S, Samali A, and Agostinis P (2012). PERK is required at the ER-mitochondrial contact sites to convey apoptosis after ROS-based ER stress. Cell Death Differ. 19, 1880–1891. [PubMed: 22705852]

Vieira HL, Haouzi D, El Hamel C, Jacotot E, Belzacq AS, Brenner C, and Kroemer G (2000). Permeabilization of the mitochondrial inner membrane during apoptosis: impact of the adenine nucleotide translocator. Cell Death Differ. 7, 1146–1154. [PubMed: 11175251]

Wang X, Wen Y, Dong J, Cao C, and Yuan S (2018). Systematic In-Depth Proteomic Analysis of Mitochondria-Associated Endoplasmic Reticulum Membranes in Mouse and Human Testes. Proteomics 18, e1700478. [PubMed: 29785746]

Wei MC, Zong WX, Cheng EH, Lindsten T, Panoutsakopoulou V, Ross AJ, Roth KA, MacGregor GR, Thompson CB, and Korsmeyer SJ (2001). Proapoptotic BAX and BAK: a requisite gateway to mitochondrial dysfunction and death. Science 292, 727–730. [PubMed: 11326099]

White C, Li C, Yang J, Petrenko NB, Madesh M, Thompson CB, and Foskett JK (2005). The endoplasmic reticulum gateway to apoptosis by Bcl-X(L) modulation of the InsP3R. Nat. Cell Biol 7, 1021–1028. [PubMed: 16179951]

Wieckowski MR, Giorgi C, Lebiedzinska M, Duszynski J, and Pinton P (2009). Isolation of mitochondria-associated membranes and mitochondria from animal tissues and cells. Nat. Protoc 4, 1582–1590. [PubMed: 19816421]

Zhang A, Williamson CD, Wong DS, Bullough MD, Brown KJ, Hath-out Y, and Colberg-Poley AM (2011). Quantitative proteomic analyses of human cytomegalovirus-induced restructuring of endoplasmic reticulum-mitochondrial contacts at late times of infection. Mol. Cell. Proteomics 10, M111.009936.

Highlights

- BOK interacts with the IP3Rs in mitochondria-associated membranes (MAMs)
- BOK potentiates ER-mitochondrial contact sites and protein expression in MAMs
- BOK regulates Ca^{2+} transfer from the ER to the mitochondria
- The transfer of Ca^{2+} at MAMs by BOK is an apoptotic control point

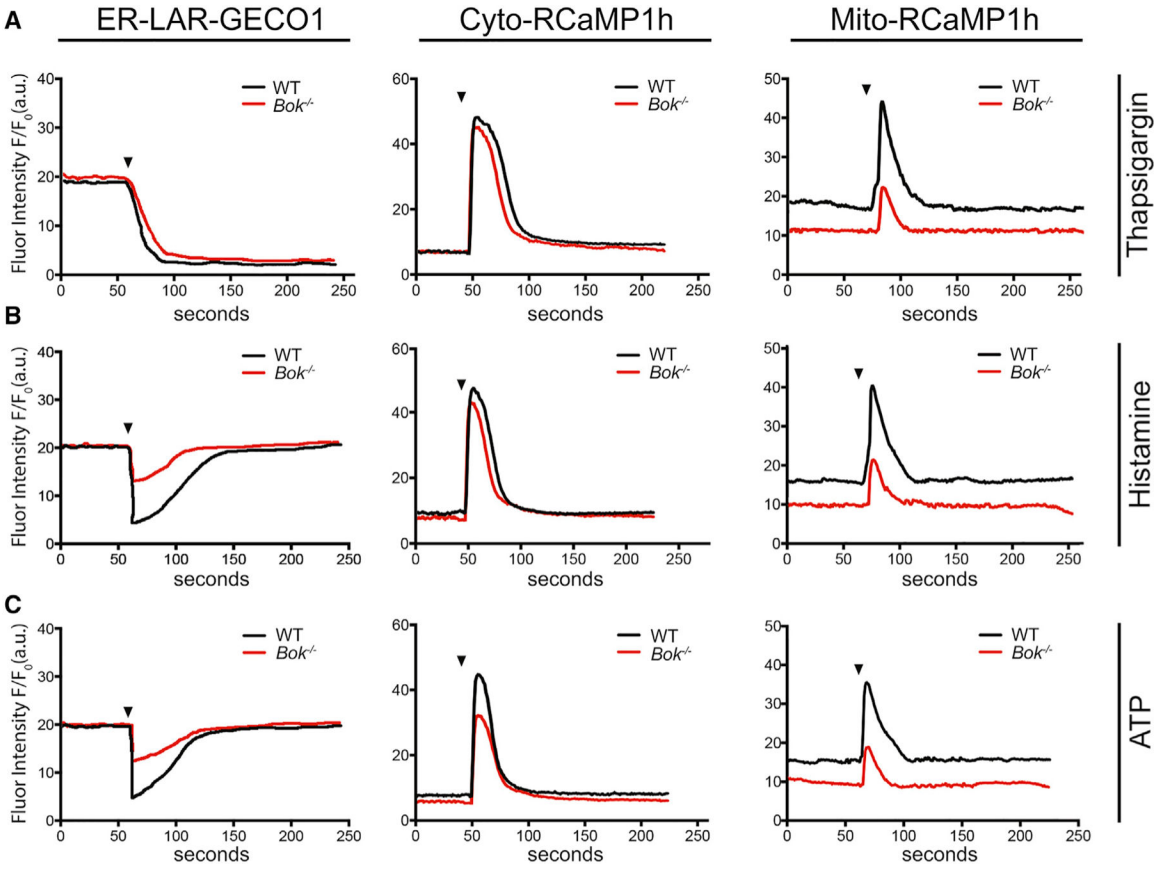

Figure 1. BOK is necessary for the transfer of Ca^{2+} from the ER to the mitochondria

(A–C) Relative fluorescence intensity (y axis) is measured over time (x axis) in defined regions of interest in WT and *Bok*$^{-/-}$ MEFs by the genetically encoded Ca^{2+} indicators ER-LAR-GECO1 for the endoplasmic reticulum (ER) (first column), Cyto-RCaMP1h for the cytoplasm (second column), or Mito-RCaMP1h for the mitochondria (third column). Cells were treated at 50 s (arrowhead) with either (A) 2 μM thapsigargin, (B) 100 μM histamine, or (C) 10 μM ATP. A representative curve from at least three independent experiments is plotted. Measurements were made on at least 5 fields with more than 8–10 cells per field (at least 50–60 cells total) for each condition within each experiment.

See also Figure S1.

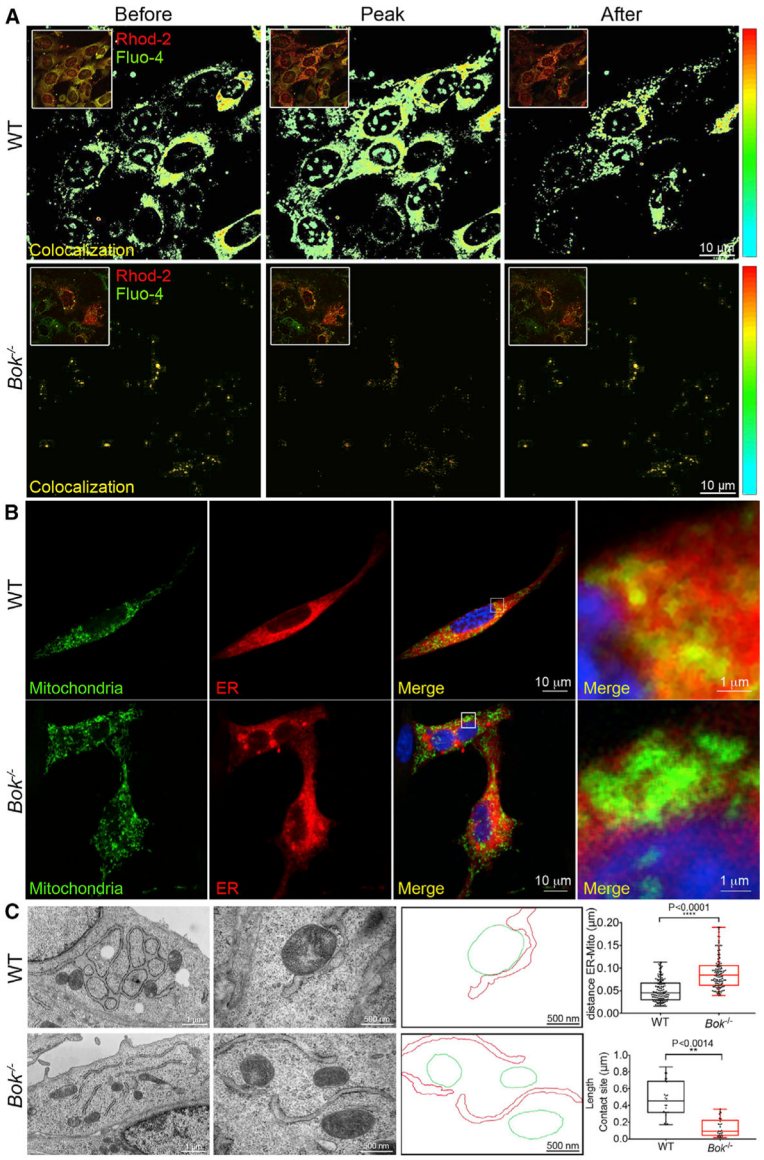

Figure 2. Mitochondrial-ER contact points are decreased in the absence of BOK

(A) Quantified co-localization (Pearson correlation coefficient > 0.65) intensity of Rhod-2 and Fluo-4 in WT (top) and *Bok*$^{-/-}$ (bottom) MEFs, 30 s before (left), at the peak of co-localization (middle), and 30 s after (right) treatment with 2 μM thapsigargin. Scale for intensity of merge is shown on the right. The inset shows fluorescence for the Rhod-2 and Fluo-4 channels.

(B) Confocal microscopy of WT (top) and *Bok*$^{-/-}$ (bottom) MEFs, transiently expressing pShooter-Mito-GFP (first column) and mRFP-FRB-9x-ER (second column). An image of their merge along with SYTOX-Deep-Red-stained nuclei false-colored blue is shown in the third column, with a higher magnification of the white boxed region in the third column shown in the fourth column. Yellow indicates overlap. Scale bar for the first three columns is shown in the third column and represents 10 μm, whereas the scale bar for the fourth column represents 1 μm.

(C) Representative transmission electron micrographic (EM) images of WT (top) and *Bok*$^{-/-}$ (bottom) MEFs at low (first column) and high (second column) power. Third column shows bounding image of the second column with mitochondria in green and ER in red as completed in ImageJ. The top scatterplot in the fourth column shows the distance between the mitochondria and ER in WT (n = 125 sites) and *Bok*$^{-/-}$ (n = 117 sites) MEFs from more than 30 EM images. The bottom scatterplot in the fourth column shows the length of each contact site for those that are less than 15 nm between the ER and mitochondria in WT (n = 27) and *Bok*$^{-/-}$ (n = 25) MEFs. Data are represented as individual values and mean ± SD. Significance was calculated using an ANOVA test.
See also Figure S2.

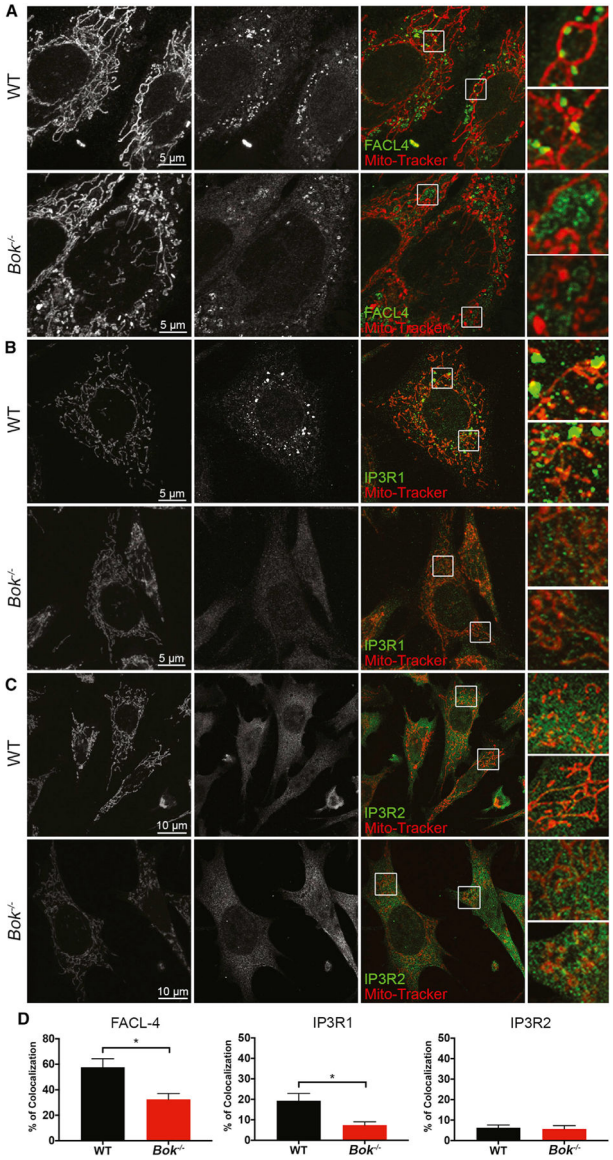

Figure 3. Mitochondria-associated membrane (MAM) proteins are mis-localized in the absence of BOK by immunofluorescence

(A–C) Localization in a single plane by confocal microscopy of MitoTracker (first column) with respect to (A) FACL-4, (B) IP3R1, and (C) IP3R2 (second column). The merged image is shown at low (third column) and high (fourth column) power. (D) Quantification of percent co-localization of the individual protein with MitoTracker in 20–30 images per condition from three independent experiments. Data are represented as mean ± SD. Significance was calculated using an ANOVA test (*$p < 0.05$).

See also Figure S3.

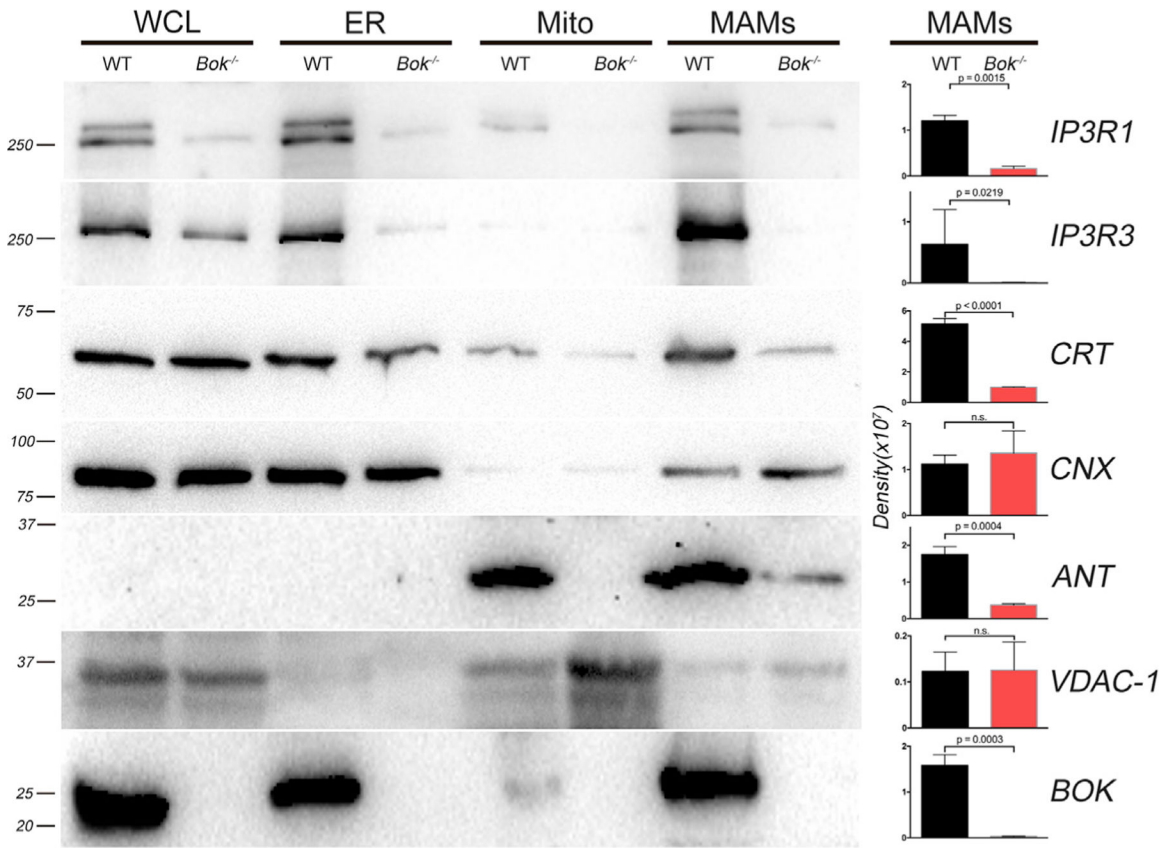

Figure 4. MAM proteins are reduced in the absence of BOK by biochemical fractionation

Representative western blot analysis (n = at least 3) for mitochondrial, bulk ER, and MAM proteins in WT and *Bok*$^{-/-}$ MEFs. Equal total protein was loaded for each fraction (20 μg for IP3R1, 20 μg for IP3R3, 10 μg for CRT, 10 μg for CNX, 40 μg for ANT, 40 μg for VDAC1, and 30 μg for BOK). Molecular weight markers are shown in kDa on the left. Density of the bands in the MAMs was quantified with a Bio-Rad ChemiDoc and plotted on the right. Data are represented as mean ± SD. Significance was calculated using an ANOVA test (ns, non-significant). CNX, calnexin; CRT, calreticulin; Mito, mitochondria; WCL, whole-cell lysate.

See also Figure S4.

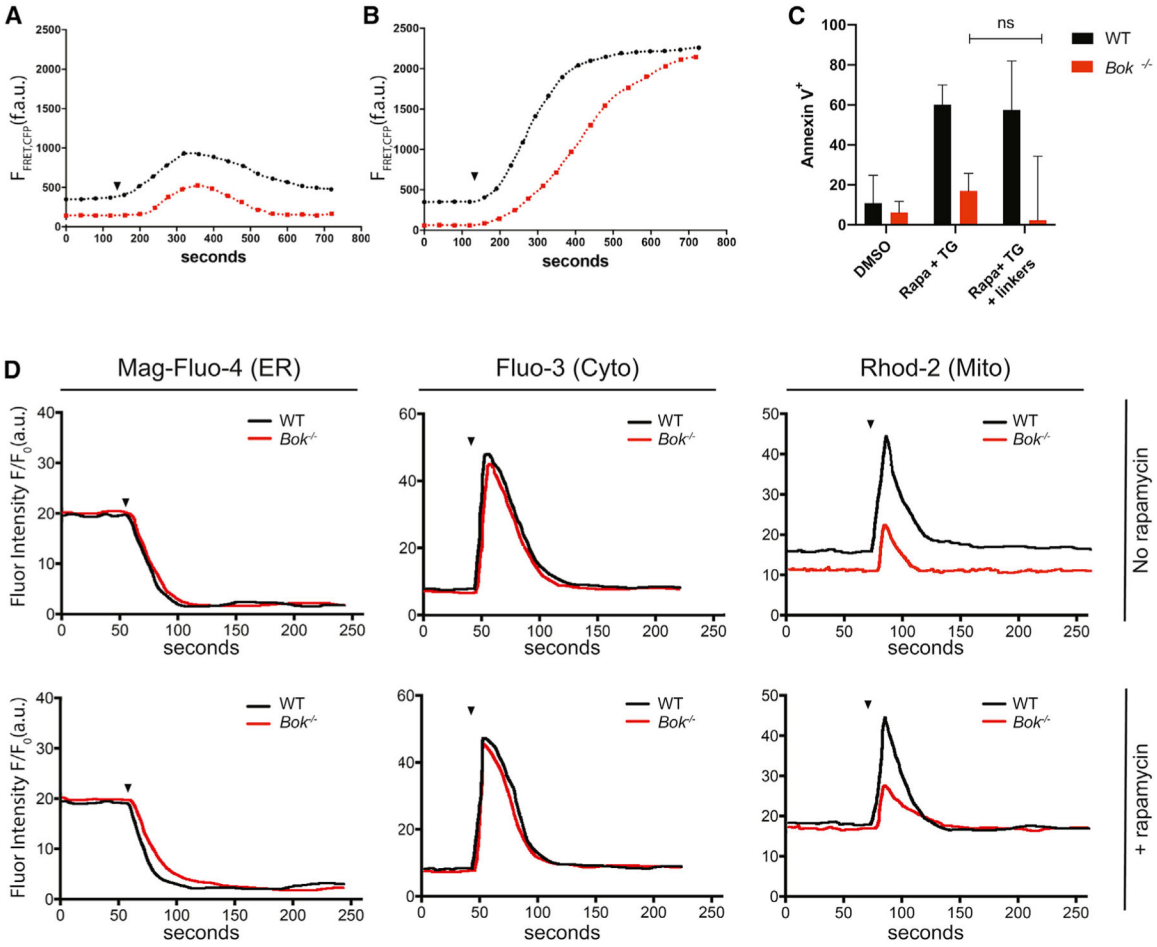

Figure 5. Restoration of ER-mitochondrial proximity without BOK does not rescue apoptosis or stimulus-induced Ca^{2+} transfer

(A) Time course of FRET fluorescence during early treatment with 2 μM thapsigargin (arrowhead) in WT and *Bok*$^{-/-}$ cells.

(B) Time course of FRET fluorescence during induction of the linkage by 100 nM rapamycin (arrowhead).

(C) Percent annexin-V-positive WT and *Bok*$^{-/-}$ cells treated with DMSO (DMSO), treated with 100 nM rapamycin for 10 min followed by fresh media containing 2 μM thapsigargin for 16 h (Rapa + TG) after mock transfection, or transiently transfected with the plasmid and treated with rapamycin and thapsigargin (Rapa +TG + linkers). Data are represented as mean ± SD. Significance was calculated using an ANOVA test (ns, not significant).

(D) Fluorescence intensity is measured in defined regions of interest in WT and *Bok*$^{-/-}$ MEFs by the Ca^{2+} indicator dyes Mag-Fluo-4 for the ER (first column), Fluo-3 for the cytoplasm (second column), or Rhod-2 for the mitochondria (third column). Cells were untreated (top row) or treated with 100 nM rapamycin (bottom row) for 10 min before being treated with 2 μM thapsigargin (arrowhead). A representative curve from at least three independent experiments is plotted. Measurements were made on at least 5 fields with more than 8–10 cells per field (at least 50–60 cells total) for each condition within each experiment.

See also Figure S5.

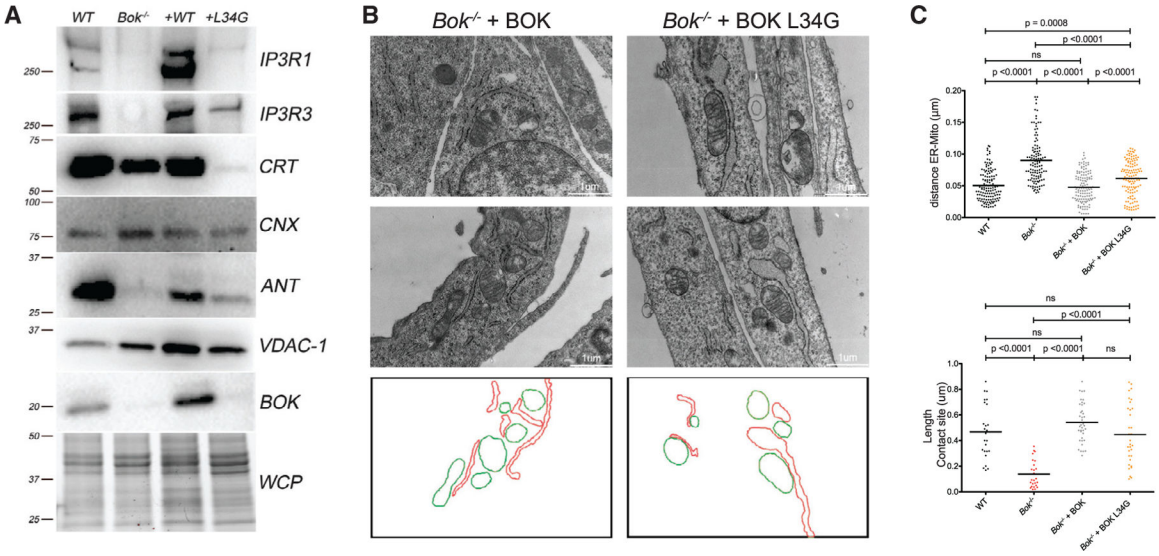

Figure 6. Disruption of the BOK-IP3R interaction decreases MAM proteins with minimal impact on ER-mitochondrial apposition

(A) Representative western blot analysis (n = at least 3) for MAM proteins in WT and *Bok*$^{-/-}$ MEFs as well as *Bok*$^{-/-}$ MEFs with stable expression of WT FLAG-BOK (+WT) or L34G FLAG-BOK (+L34G). Equal total protein was loaded for each fraction as described in Figure 4. Molecular weight markers are shown in kDa on the left.

(B) Representative transmission EM images of *Bok*$^{-/-}$ MEFs stably transfected with WT (left) or L34G (right) FLAG-BOK. The bottom row shows bounding image of the middle row with mitochondria in red and ER in green as completed in ImageJ.

(C) The top scatterplot shows the distance between the mitochondria and ER in WT (n = 125 sites), *Bok*$^{-/-}$ (n = 117 sites), *Bok*$^{-/-}$ + WT FLAG-BOK (n = 127 sites), and *Bok*$^{-/-}$ + L34G FLAG-BOK (n = 124 sites) MEFs from more than 30 EM images. The bottom scatterplot shows the length of each contact site for those that are less than 15 nm between the ER and mitochondria in WT (n = 27), *Bok*$^{-/-}$ (n = 25), *Bok*$^{-/-}$ + WT FLAG-BOK (n = 38), and *Bok*$^{-/-}$ + L34G FLAG-BOK (n = 32) MEFs. WT and *Bok*$^{-/-}$ MEF data are from Figure 2C. Data are represented as individual values and mean (bar). Significance was calculated using an ANOVA test (ns, not significant).

See also Figure S6.

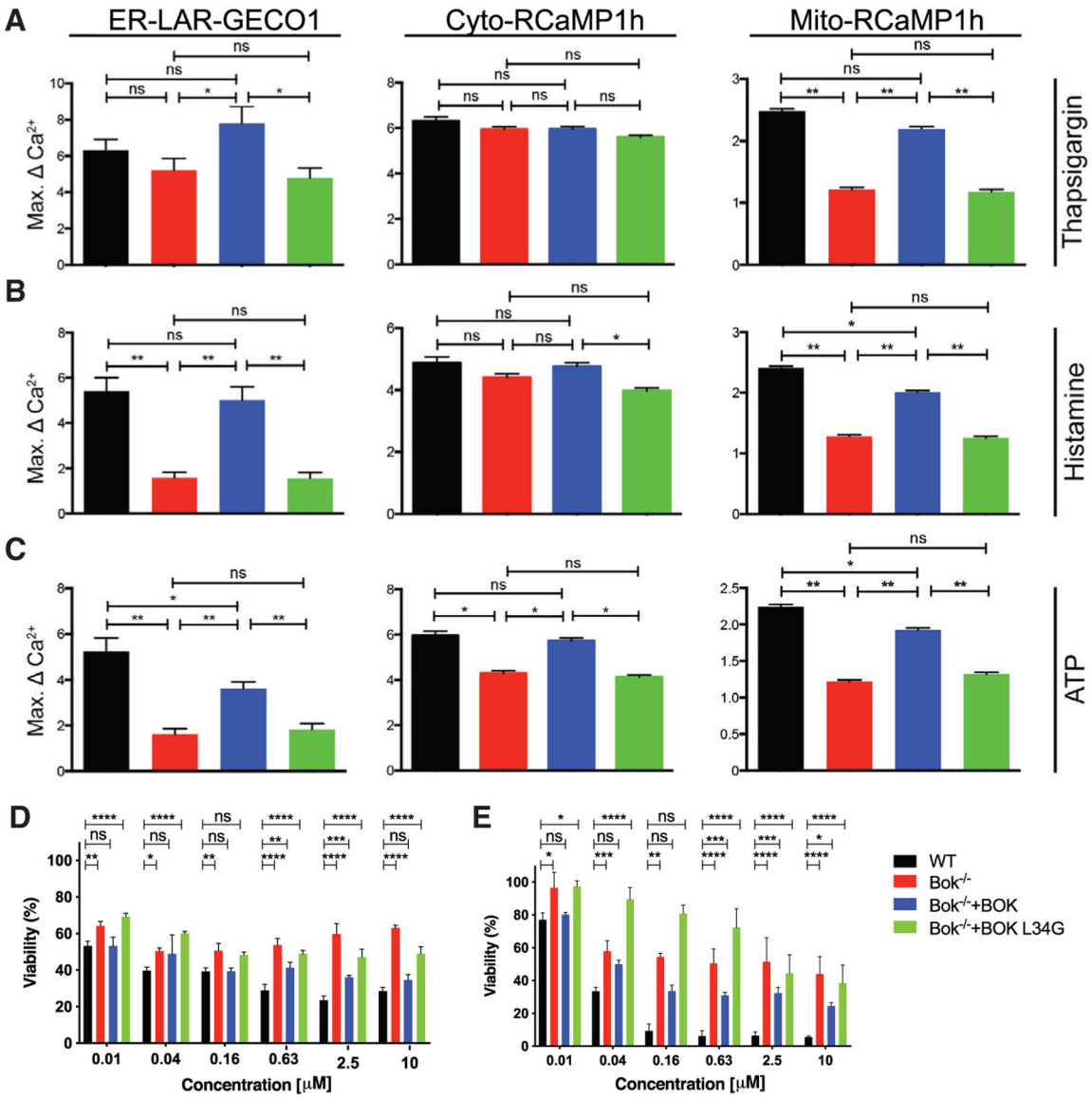

Figure 7. Disruption of the BOK-IP3R interaction attenuates Ca^{2+} transfer from the ER to the mitochondria and apoptosis

(A–C) Fluorescence intensity is measured in defined regions of interest in WT, *Bok*$^{-/-}$, *Bok*$^{-/-}$ + WT FLAG-BOK, and *Bok*$^{-/-}$ + L34G FLAG-BOK MEFs by the genetically encoded Ca^{2+} indicators ER-LAR-GECO1 for the ER (first column), Cyto-RCaMP1h for the cytoplasm (second column), or Mito-RCaMP1h for the mitochondria (third column). Cells were treated at 50 s with either (A) 2 μM thapsigargin, (B) 100 μM histamine, or (C) 10 μM ATP. The average maximum fold change from the baseline in three independent experiments is shown with a representative curve plotted in Figure S7. Measurements were made on at least 5 fields with more than 8–10 cells per field (at least 50–60 cells total) for each condition within each experiment. WT and *Bok*$^{-/-}$ MEF data are from Figure 1.

(D and E) Cell viability was measured at 24 h by XTT for WT MEFs, *Bok*$^{-/-}$ MEFs, and *Bok*$^{-/-}$ MEFs stably transfected with WT or L34G FLAG-BOK treated with thapsigargin

(D) or bortezomib (E). Data are represented as mean ± SD. Significance was calculated using an ANOVA test (ns, *p < 0.05, **p < 0.01, ***p < 0.001, ****p < 0.0001).
See also Figure S7.

KEY RESOURCES TABLE

REAGENT or RESOURCE	SOURCE	IDENTIFIER
Antibodies		
Rabbit polyclonal anti-FACL-4	Abcam	ab38420; RRID: AB_2222536
Rabbit polyclonal anti-Sigma-1	Abcam	Ab53852; RRID: AB_881796
Rabbit polyclonal Anti-IP3R1	Invitrogen	PA1–901; RRID: AB_2129984
Rabbit monoclonal Anti-IP3R1	Cell Signaling	8568; RRID: AB_10890699
Goat polyclonal Anti-IP3R1	Santa Cruz	sc6093; RRID: AB_649542
Goat polyclonal Anti-IP3R2	Santa Cruz	sc7278; RRID: AB_2265201
Mouse monoclonal Anti-IP3R2	Santa Cruz	sc398434
Mouse monoclonal Anti-IP3R3	BD Biosciences	610312; RRID: AB_39704
Mouse monoclonal Anti-ANT	Mitosciences	MSA02; RRID: AB_478281
Mouse monoclonal Anti-ANT	Abcam	ab110322; RRID: AB_10862212
Alexa Fluor 488-conjugated goat anti-mouse IgG	Molecular Probes	A-11001; RRID: AB_2534069
Alexa Fluor 546-conjugated goat anti-mouse IgG	Molecular Probes	A-11030; RRID: AB_144695
Mouse monoclonal Anti-Calreticulin	BD Biosciences	612136; RRID: AB_399507
Mouse monoclonal Anti-Calnexin	Santa Cruz	SC-46669; RRID: AB_626784
Rabbit polyclonal Anti-VDAC1	ThermoFisher	PA1–954A; RRID: AB_2304154
Mouse monoclonal Anti-VDAC1	Santa Cruz	sc390996; RRID: AB_2750920
Rabbit polyclonal Anti-VDAC1/2/3	Santa Cruz	sc98708; RRID: AB_2214795
Rabbit monoclonal Anti-FLAG	Sigma-Aldrich	F7425; RRID: AB_439687
Rabbit monoclonal Anti-BOK	Abcam	Ab233072
Rabbit monoclonal Anti-BOK	Abcam	Ab186745; RRID: AB_2728737
Rabbit polyclonal Anti-BOK	Abcam	Ab130344; RRID: AB_11155461
Chemicals, peptides, and recombinant proteins		
Fluo-3 acetoxymethyl ester	Thermo Fisher	F1241
Mag-Fluo-4 acetoxymethyl ester	Thermo Fisher	M14206
Rhod-2 acetoxymethyl ester	Thermo Fisher	R1245MP
Thapsigargin	Sigma-Aldrich	T9033
Bortezomib	EMD Millipore Corporation	5.04314.0001
Histamine	Sigma-Aldrich	H7125
ATP	Sigma-Aldrich	A1852
ER-Tracker Green	Molecular probes	E34251
MitoTracker Deep Red FM	Molecular probes	M22426
TO-PRO-3 far red	Molecular probes	T3605
MitoTracker CMTMRos Orange	Molecular probes	M7510
Rapamycin	Invitrogen	Tlrl-rap
Tert-Butylhydroquinone	Sigma-Aldrich	112941
Critical commercial assays		
XTT Cell viability kit	Cell Signaling Tech.	9095S
PE/Cy7 Annexin V	BioLegend	640949
MitoStatus TMRE	BD PharMingen	564696; RRID: AB_2869606

REAGENT or RESOURCE	SOURCE	IDENTIFIER
Experimental models: cell lines		
WT MEF cells, SV-40 immortalized	This paper	N/A
Bok KO MEF cells, SV-40 immortalized	This paper	N/A
Recombinant DNA		
Plasmid: YFP-FKBP-Mito targeting	Gift from Gyorgy Hajnóczky	N/A
Plasmid: CFP-FRB-ER targeting	Gift from Gyorgy Hajnóczky	N/A
Plasmid: Pericam-FKBP-Mito targeting	Gift from Gyorgy Hajnóczky	N/A
Plasmid: RFP-FRB-short-ER targeting	Gift from Gyorgy Hajnóczky	N/A
Plasmid: RFP-FRB-long-ER targeting	Gift from Gyorgy Hajnóczky	N/A
Plasmid: FEMP	Gift from Luca Scorrano	N/A
Plasmid: pShooter Mito-GFP	Invitrogen	V82220
Plasmid: ER-LAR-GECO1	Addgene	61244; RRID: Addgene_61244
Plasmid: Cyto-RCaMP1h	Addgene	105014; RRID: Addgene_105014
Plasmid: Mito-RCaMP1h	Addgene	105013; RRID: Addgene_105013
Plasmid: pMIG-FLAG-HA-BOK WT-IRES-GFP	This paper	N/A
Plasmid: pMIG-FLAG-HA-BOK L34G-IRES-GFP	This paper	N/A